

## Identification of a Potent, Highly Selective, and Brain Penetrant Phosphodiesterase 2A Inhibitor Clinical Candidate

Christopher J. Helal, Eric P Arnold, Tracey L Boyden, Cheng Chang, Thomas A. Chappie, Ethan Fisher, Mihaly Hajós, John F. Harms, William E. Hoffmann, John M. Humphrey, Jayvardhan Pandit, Zhijun Kang, Robin J. Kleiman, Bethany L. Kormos, Che-Wah Lee, Jiemin Lu, Noha Maklad, Laura McDowell, Dina McGinnis, Rebecca E O'Connor, Christopher J. O'Donnell, Adam Ogden, Mary Piotrowski, Christopher J. Schmidt, Patricia Seymour, Hirokazu Ueno, Nichole Vansell, Patrick R. Verhoest, and Edward X. Yang

*J. Med. Chem.*, **Just Accepted Manuscript** • DOI: 10.1021/acs.jmedchem.7b01466 • Publication Date (Web): 02 Jan 2018

Downloaded from <http://pubs.acs.org> on January 3, 2018

### Just Accepted

“Just Accepted” manuscripts have been peer-reviewed and accepted for publication. They are posted online prior to technical editing, formatting for publication and author proofing. The American Chemical Society provides “Just Accepted” as a free service to the research community to expedite the dissemination of scientific material as soon as possible after acceptance. “Just Accepted” manuscripts appear in full in PDF format accompanied by an HTML abstract. “Just Accepted” manuscripts have been fully peer reviewed, but should not be considered the official version of record. They are accessible to all readers and citable by the Digital Object Identifier (DOI®). “Just Accepted” is an optional service offered to authors. Therefore, the “Just Accepted” Web site may not include all articles that will be published in the journal. After a manuscript is technically edited and formatted, it will be removed from the “Just Accepted” Web site and published as an ASAP article. Note that technical editing may introduce minor changes to the manuscript text and/or graphics which could affect content, and all legal disclaimers and ethical guidelines that apply to the journal pertain. ACS cannot be held responsible for errors or consequences arising from the use of information contained in these “Just Accepted” manuscripts.

1  
2  
3  
4  
5  
6  
7  
8  
9  
10  
11  
12  
13  
14  
15  
16  
17  
18  
19  
20  
21  
22  
23  
24  
25  
26  
27  
28  
29  
30  
31  
32  
33  
34  
35  
36  
37  
38  
39  
40  
41  
42  
43  
44  
45  
46  
47  
48  
49  
50  
51  
52  
53  
54  
55  
56  
57  
58  
59  
60

1  
2  
3  
4  
5  
6  
7 Identification of a Potent, Highly Selective, and  
8  
9  
10  
11 Brain Penetrant Phosphodiesterase 2A Inhibitor  
12  
13  
14  
15 Clinical Candidate  
16  
17  
18  
19

20 *Christopher J. Helal,\* Eric Arnold,<sup>a</sup> Tracey Boyden,<sup>a</sup> Cheng Chang,<sup>a</sup> Thomas A. Chappie,<sup>b</sup>*  
21 *Ethan Fisher,<sup>a</sup> Mihaly Hajos,<sup>a</sup> John F. Harms,<sup>b</sup> William E. Hoffman,<sup>a</sup> John M. Humphrey,<sup>a</sup>*  
22 *Jayvardhan Pandit,<sup>a</sup> Zhijun Kang,<sup>a</sup> Robin J. Kleiman,<sup>a</sup> Bethany L. Kormos,<sup>b</sup> Che-Wah Lee,<sup>a</sup>*  
23 *Jiemin Lu,<sup>a</sup> Noha Maklad,<sup>a</sup> Laura McDowell,<sup>a</sup> Dina McGinnis,<sup>a</sup> Rebecca E. O'Connor,<sup>a</sup>*  
24 *Christopher J. O'Donnell,<sup>a</sup> Adam Ogden,<sup>a</sup> Mary Piotrowski,<sup>a</sup> Christopher J. Schmidt,<sup>b</sup> Patricia*  
25 *A. Seymour,<sup>a</sup> Hirokazu Ueno,<sup>a</sup> Nichole Vansell,<sup>a</sup> Patrick R. Verhoest,<sup>b</sup> and Edward X. Yang<sup>a</sup>*  
26  
27  
28  
29  
30  
31  
32  
33  
34

35 <sup>a</sup>Pfizer Worldwide Research and Development, Eastern Point Road, Groton, CT 06340

36 <sup>b</sup>Pfizer Worldwide Research and Development, 1 Portland Street, Cambridge, MA 02139

37  
38  
39  
40 KEYWORDS: phosphodiesterase (PDE) 2A, cyclic guanosine monophosphate (cGMP), N-  
41 methyl-D-aspartate receptor antagonist, ketamine, MK-801, cortical EEG, modified release  
42  
43  
44 formulation  
45  
46  
47  
48  
49  
50

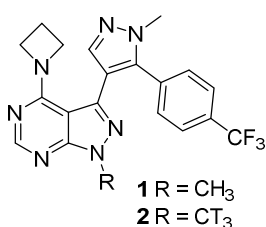
51 ABSTRACT. Computational modeling was used to direct the synthesis of analogs of previously  
52 reported phosphodiesterase 2A (PDE2A) inhibitor **1** with an imidazotriazine core to yield  
53 compounds of significantly enhanced potency. The analog PF-05180999 (**30**) was subsequently  
54  
55  
56  
57  
58  
59  
60

1  
2  
3 identified as a pre-clinical candidate targeting cognitive impairment associated with  
4 schizophrenia. Compound **30** demonstrated potent binding to PDE2A in brain tissue, dose  
5 responsive mouse brain cGMP increases, and reversal of *N*-methyl-D-aspartate (NMDA)  
6 antagonist-induced (MK-801, ketamine) effects in electrophysiology and working memory  
7 models in rats. Pre-clinical pharmacokinetics revealed unbound brain/unbound plasma levels  
8 approaching unity and good oral bioavailability resulting in an average concentration at steady  
9 state ( $C_{av,ss}$ ) predicted human dose of 30 mg once daily (QD). Modeling of a modified release  
10 formulation suggested that 25 mg twice daily (BID) could maintain plasma levels of **30** at or  
11 above targeted efficacious plasma levels for 24 hrs. which became part of the human clinical  
12 plan.  
13  
14  
15  
16  
17  
18  
19  
20  
21  
22  
23  
24  
25

### 26 27 *Introduction*

28  
29  
30 Phosphodiesterases (PDEs) play a central role in modulating cellular levels of the key second  
31 messenger molecules cGMP and cAMP. Inhibition of PDEs as a means to selectively increase  
32 discrete pools of cGMP and/or cAMP has emerged as strategy to treat a diverse set of human  
33 medical conditions such as heart failure (PDE3 inhibitors), chronic obstructive pulmonary  
34 disease, psoriatic arthritis (PDE4 inhibitors), and pulmonary hypertension and erectile  
35 dysfunction (PDE5 inhibitors). We had a particular interest in identifying inhibitors of  
36 phosphodiesterase 2A (PDE2A), a PDE that hydrolyzes both cGMP and cAMP, to treat  
37 cognitive disorders. This approach was based upon the enrichment of PDE2A in striatum,  
38 frontal cortex, and hippocampus,<sup>1</sup> brain circuitry critical for selecting and enabling cognitive  
39 programs, working memory and executive function. Additionally, data from rodent models  
40 demonstrated efficacy for PDE2A inhibitors in different models of cognition.<sup>2,3</sup> We recently  
41 disclosed the potency, selectivity, pharmacokinetics, and pharmacology of a series of PDE2A  
42  
43  
44  
45  
46  
47  
48  
49  
50  
51  
52  
53  
54  
55  
56  
57  
58  
59  
60

1  
2  
3 inhibitors represented by **1** (Figure 1), a pyrazolopyrimidine derivative.<sup>4</sup> This data provided  
4  
5 support for PDE2A inhibition as a potential treatment for cognitive impairment associated with  
6  
7 schizophrenia (CIAS), a condition that is associated with hypoglutamatergic signaling, based  
8  
9 upon the ability of **1** to reverse the effects of *N*-methy-D-aspartate (NMDA) antagonists, MK-  
10  
11 801 and ketamine, in two different *in vivo* rodent models. The exquisite PDE2A selectivity is  
12  
13 proposed to be driven by the *p*-trifluoromethyl phenyl inducing and occupying a pocket unique  
14  
15 to PDE2A (Figure 2).<sup>5,6</sup>  
16  
17  
18



27 PDE2A IC<sub>50</sub> = 2 nM  
28 PDE2A striatal binding (**2**) K<sub>d</sub> = 3 nM  
29 PDE1,3-11 selectivity >2500  
30 HLM Cl<sub>int</sub> = 85 ml/min/kg  
31 MDR BA/AB = 1.4  
32 C<sub>bu</sub>/C<sub>pu</sub> = 0.36 (rat)  
33 C<sub>bu</sub> cGMP E50, striatum = 15 nM (mouse)  
34 C<sub>bu</sub> efficacy Ketamine RAM = 2.3 - 7 nM (rat)  
35 C<sub>bu</sub> 80% effect MK-801 Cortical EEG = 11 nM (rat)  
36

37 Figure 1. Profile of **1**, a potent, selective, brain penetrant, *in vivo* active PDE2A inhibitor.<sup>4</sup> HLM

38  
39 Cl<sub>int</sub> = intrinsic clearance apparent scaled determined from human liver microsomes (HLM); MDR  
40  
41 BA/AB = ratio of basolateral-to-apical/apical-to-basolateral flux in Madin-Darby Canine Kidney  
42  
43 (MDCK) cells transfected with the multidrug-resistance gene (MDR1) that encodes for human P-  
44  
45 glycoprotein (P-gp).<sup>7</sup> C<sub>bu</sub> = unbound brain concentration. C<sub>pu</sub> = unbound plasma concentration.  
46  
47  
48  
49  
50  
51  
52  
53  
54  
55  
56  
57  
58  
59  
60

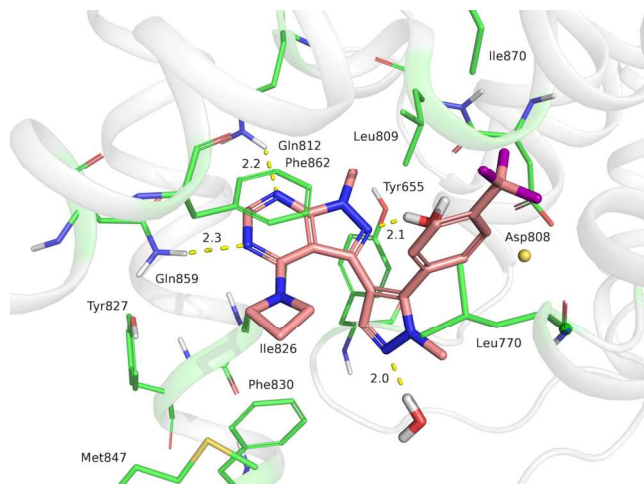


Figure 2. Model of **1** bound to PDE2A based on x-ray structure PDB 5U7L with *p*-trifluoromethylphenyl filling induced pocket.

While **1** met our target for potency, selectivity, and brain penetration for a pre-clinical candidate, we sought to reduce the estimated human dose (108 mg/day). The design strategy was to reduce HLM  $Cl_{int}$  by targeting compounds of reduced lipophilicity as measured by shake flask logD (SFlogD) (SFlogD of **1** = 2.9), while maintaining or improving the high potency and low MDR BA/AB efflux associated with **1**.

### Results

Estimated human dose for a brain targeting compound (Equation 1a) was used as a multi-parameter optimization tool as compounds with lower human doses have been reported to be less susceptible to idiosyncratic toxicology findings.<sup>8</sup> *In vitro* data surrogates were used in place of more labor intensive *in vivo* data to drive rapid decisions (Equation 1b) as described previously.<sup>4</sup>

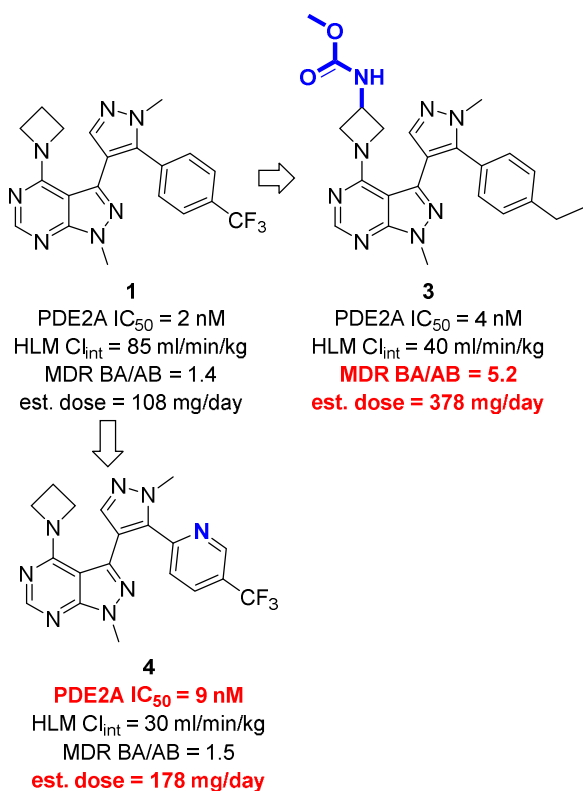
$$\text{a) Estimated human dose, } in\ vivo\ data = (C_{ss,av,bu} / (C_{bu}/C_{pu})) \times Cl_{int} \times 24\ h \times 70\ kg / Fa$$

$$\text{b) Estimated human dose, } in\ vitro\ data = (10 \times PDE2A\ IC_{50} \times MDR\ BA/AB) \times HLM\ Cl_{int} \times 24\ h \times 70\ kg$$

Equation 1. *In vivo* and *in vitro* human estimated dose equations

1  
2  
3 a)  $C_{ss,av bu}$  = targeted average unbound steady state brain concentrations of drug;  $C_{bu}/C_{pu}$  = unbound brain  
4 concentration/unbound plasma concentration;  $Cl_{int}$  = intrinsic clearance;  $F_a$  = fraction absorbed of the  
5 drug. b) MDR BA/AB = ratio of basolateral-to-apical/apical-to-basolateral flux in Madin-Darby Canine  
6 Kidney (MDCK) cells transfected with the multidrug-resistance gene (MDR1) that encodes for human P-  
7 glycoprotein (P-gp); HLM  $Cl_{int}$  = intrinsic clearance apparent scaled determined from human liver  
8 microsomes (HLM).  
9  
10  
11  
12  
13  
14  
15

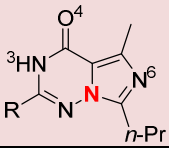
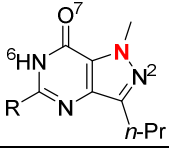
16  
17 Previous attempts to reduce lipophilicity in this series by incorporating azetidine derivatives  
18 with polar appendages preserved PDE2A potency and afforded HLM  $Cl_{int}$  reductions (Figure 3,  
19 3),<sup>4</sup> but significant, undesirable MDR BA/AB efflux was introduced. Alternatively, conversion  
20 of the pendant *p*-substituted phenyl group into a heterocycle did reduce HLM  $Cl_{int}$  and retained  
21 low MDR BA/AB efflux, but PDE2A potency suffered (4).  
22  
23  
24  
25  
26  
27

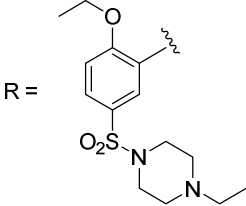


54 Figure 3. Attempts to reduce HLM  $Cl_{int}$  by reducing lipophilicity.  
55  
56  
57  
58  
59  
60

Subtle variations to the 1-methyl-1H-pyrazolo[3,4-d]pyrimidine core that would maintain key protein-ligand contacts were next considered. Realization of a potency increase without altering overall PDE selectivity and physical properties could allow for polarity enhancements of the azetidine or pendant *p*-substituted aryl groups to align potency with desirable ADME properties. We were inspired by a PDE5A example wherein alternative bicyclic cores provided differential potency.<sup>9</sup> For example, the PDE5A inhibitor vardenafil (**5**) is ca. 50x more potent than isomeric **6**, these compounds differing only by the juxtaposition of atoms in the bicyclic core that do not make direct polar interactions with the PDE5A enzyme (Table 1).<sup>10,11</sup>

Table 1. Impact of atom position on potency differences in **5** and **6**

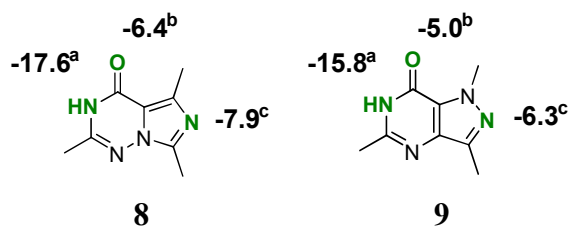
ID		PDE5A IC <sub>50</sub> (nM)
<b>5</b>		0.17
<b>6</b>		8.9

R = 

We undertook a computational approach to see if the potency differences between **5** and sildenafil (**7**) (**6** with *N*-methyl vs. *N*-ethyl piperazine) could be explained by differential hydrogen bonding interactions between the bicyclic cores and the PDE5A protein, with the ultimate goal of predicting potency increases for our proposed PDE2A inhibitors.<sup>12</sup> The X-ray co-crystal structures of **5** and **7** with the catalytic domain of PDE5A (Protein Data Bank (PDB)

IDs 1XP0 and 1TBF, respectively) indicate that the imidazotriazinone and pyrazolopyrimidinone bicyclic cores make hydrogen bond interactions with Gln817 (N(H)-3 and C(O)-4 in **5** and N(H)-6 and C(O)-7 in **7**), Gln775 (water-mediated through C(O)-4 in **5** and C(O)-7 in **7**) and Tyr612 sidechain/Asp764 backbone carbonyl (water-mediated through N-6 in **5** and N-2 in **7**). Hydrogen bond strength calculations were computed for each individual residue or water interaction with truncated versions of **5** (**8**) and **6** (**9**) then summed to determine an overall contribution to the binding energy of these three hydrogen bond interactions (Table 2). In summary, the relative binding energies correctly rank order the compounds with respect to potency and also appear to be a reasonable approximation of the relative binding free energy difference between the two compounds based on their potencies.

Table 2. Comparison of calculated hydrogen bonding strengths of truncated bicycle cores **8** and **9** with PDE5A versus measured PDE5 IC<sub>50</sub> values for **5** and **6**

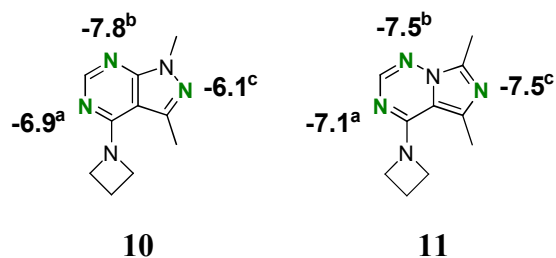


	Calculated (Truncated System)	
	$\Delta G$ (kcal/mol)	$\Delta\Delta G$ (kcal/mol)
<b>8</b>	-31.9	0.0
<b>9</b>	-27.1	4.8
Experimental		
<b>5</b>	-13.6	0.0
<b>6</b>	-11.3	2.3

(a) Calculated H-bond strength (kcal/mol) with highlighted atoms and Gln817. (b) Calculated H-bond strength (kcal/mol) with highlighted atom and structural water interacting with Gln775. (c) Calculated H-bond strength (kcal/mol) with highlighted atom and structural water molecule interacting with Tyr612 and Asp764.

Encouraged by these promising results, we calculated hydrogen bond interaction strengths for the pyrazolopyrimidine core (**10**) and an imidazotriazine core (**11**) to predict PDE2A inhibitory potency (Table 3). The X-ray crystal structure of a compound with a pyrazolopyrimidine core (PDB ID 5U7L, Figure 2) indicates that it hydrogen bonds with the conserved Gln859, Gln812 and Tyr655/Asp808 backbone carbonyl (water-mediated). As with the PDE5 cores, hydrogen bond strength calculations were computed for each individual residue or water interaction with **10** and **11**, then summed to determine an overall contribution to the binding energy of these three hydrogen bond interactions. As with the PDE5A example, these calculations suggested that **11** would have stronger hydrogen bond interactions with PDE2A versus **10**. With this potential improvement in potency, we pursued synthesis of compounds of general formula **12** (Figure 4).

Table 3. Comparison of calculated PDE2A potencies across bicyclic cores **10** and **11**



	Calculated (Truncated System)	
	$\Delta G$ (kcal/mol)	$\Delta\Delta G$ (kcal/mol)
<b>10</b>	-20.8	1.3
<b>11</b>	-22.1	0.0

See Figure 2 for protein-ligand contacts. (a) Calculated H-bond strength (kcal/mol) with highlighted atom and Gln859. (b) Calculated H-bond strength (kcal/mol) with highlighted atom and Gln812. (c) Calculated H-bond strength (kcal/mol) with highlighted atom and structural water molecule interacting with Tyr655 and Asp808.

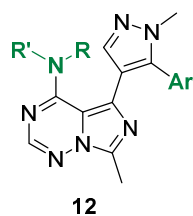


Figure 4. General imidazotriazine structure **12** targeted for synthesis

A key synthetic challenge for the imidazotriazine series was formation of the N-N bond embedded within the bicyclic core. Initial routes sought to generate this bond via amination of an imidazole (**13** to **14**, Figure 5), but yields were modest with side products and the most effective amination reagent, *O*-(4-nitrobenzoyl)hydroxylamine (**15**),<sup>13</sup> was found to be sufficiently energetic to preclude large scale usage based upon internal guidance.

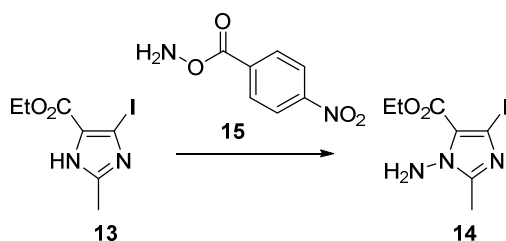


Figure 5. Amination route of **13** to **14**

To circumvent the N-N bond forming reaction, we sought an alternative disconnection with this key bond derived from commercial starting materials (Figure 6). We felt **12** could be generated from **16**, wherein X is a leaving group and R is a functional group that would facilitate introduction of the aryl/heteroaryl group. The intermediate **16** would be derived from **17** via activation of the C=O group. Imidazotriazinone **17** would originate from *N*-aminoimidazole **18**, which would derive from the condensation of  $\alpha$ -bromoketone (**19**) with a protected (PG) amidohydrazide **20**, the source of the N-N bond that ultimately originates from readily available hydrazine.<sup>14</sup>

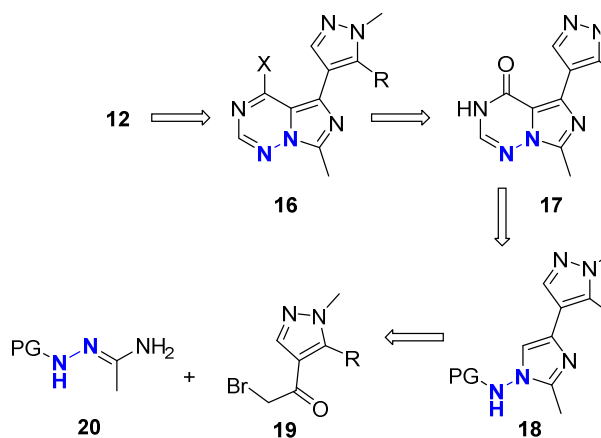
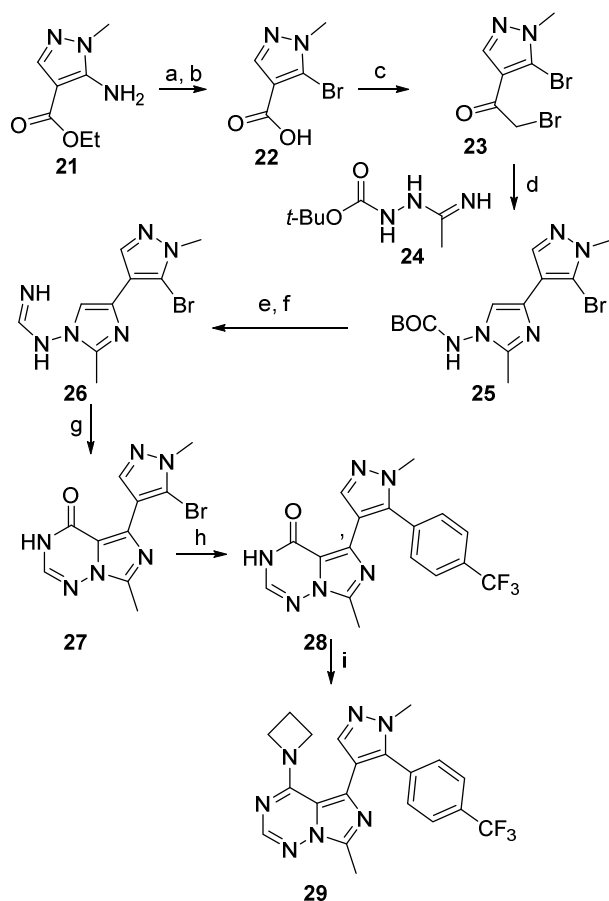


Figure 6. Alternative imidazotriazinone retro-synthesis starting with N-N bond formed.

In a forward sense, commercially available aminopyrazole **21** was converted to the 5-bromopyrazole via treatment with copper (II) bromide and *tert*-butyl nitrite followed by hydrolysis to acid **22** (Scheme 1). This was followed by transformation of **22** to the acid chloride, then treatment with trimethylsilyl diazomethane and hydrogen bromide to yield **23**. Reaction of *N*-amino amidine **24** (prepared from reaction between *tert*-butoxycarbonyl hydrazide and *O*-ethylacetimidate hydrochloride) with **23** occurred regioselectively to yield the targeted *N*-aminoimidazole **25** and thus established the critical N-N bond of the subsequent imidazotriazine ring system. Acidic removal of the BOC group followed by condensation with formamidine acetate provided amidine **26**. In order to construct the triazinone ring system, **26** was acylated with carbonyl ditriazole (CDT) and heated, likely eliminating triazole to form an isocyanate which resulted in intramolecular acylation to yield imidazotriazinone **27**. Suzuki cross-coupling with (4-(trifluoromethyl)phenyl)boronic acid afforded **28**, which was activated with POCl<sub>3</sub>/triazole, then treated with azetidine to afford **29**.



Scheme 1. Synthesis of imidazotriazine analog **29**. (a)  $\text{CuBr}_2$ , *tert*-butyl nitrite,  $\text{Et}_2\text{O}$ ,  $65\text{ }^\circ\text{C}$ , 66% (b)  $\text{LiOH}$ ,  $\text{THF}/\text{MeOH}/\text{water}$ ,  $23\text{ }^\circ\text{C}$ , 92% (c) i.  $\text{NaOMe}$ ,  $\text{MeOH}$ ;  $23\text{ }^\circ\text{C}$  ii. Oxalyl chloride,  $\text{DMF}$  (cat),  $\text{CH}_2\text{Cl}_2$ ,  $23\text{ }^\circ\text{C}$  iii.  $\text{TMS-CHN}_2$ ,  $\text{CH}_3\text{CN}$ ,  $23\text{ }^\circ\text{C}$ ;  $\text{HBr}/\text{AcOH}$ ,  $0\text{ }^\circ\text{C}$ , 78% (d)  $\text{DIPEA}$ ,  $2\text{-MeTHF}/\text{DME}$ , reflux, 59% (e)  $\text{TFA}$ ,  $\text{CH}_2\text{Cl}_2$ ,  $23\text{ }^\circ\text{C}$ , 96% (f) formamidine acetate,  $2\text{-butanol}$ ,  $100\text{ }^\circ\text{C}$ , 72% (g)  $\text{CDT}$ ,  $1,4\text{-dioxane}$ ,  $23\text{ to }50\text{ }^\circ\text{C}$ , 66% (h)  $4\text{-(trifluoromethyl)phenyl boronic acid}$ ,  $\text{Pd(dppf)Cl}_2\text{-CH}_2\text{Cl}_2$ ,  $\text{Cs}_2\text{CO}_3$ ,  $i\text{-PrOH}/\text{H}_2\text{O}$ , reflux, 58% (i) i.  $1\text{H-}1,2,4\text{-triazole}$ ,  $\text{POCl}_3$ ,  $\text{Et}_3\text{N}$ ,  $\text{CH}_2\text{Cl}_2$ ,  $70\text{ }^\circ\text{C}$ ; ii. azetidine,  $\text{Cs}_2\text{CO}_3$ ,  $\text{DMF}$ ,  $23\text{ }^\circ\text{C}$ , 85%.

The initial data with **29** showed a 5x increase in potency relative to **1** in line with computational predictions ( $\Delta\Delta\text{G}$  predicted = 1.3 kcal/mol;  $\Delta\Delta\text{G}$  experimental = 1.1 kcal/mol), but with the same SFLogD as **1**, resulting in an improved lipophilic ligand efficiency (LipE = -

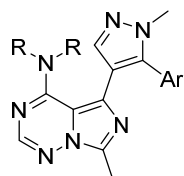
log<sub>10</sub>(PDE2A IC<sub>50</sub>) - SFLogD)<sup>15</sup> (Table 4). Additionally, similar HLM Cl<sub>int</sub> (93 ml/min/kg) and MDR BA/AB (1.6) values were observed versus **1**, suggesting that compound clearance and transporter trends would translate from the pyrazolopyrimidine series to the imidazotriazine series.

Table 4. Comparison of calculated hydrogen bond donor strengths of truncated systems (**10** and **11**) to measured  $\Delta G$  and  $\Delta\Delta G$  values for **1** and **29**.

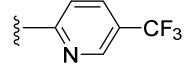
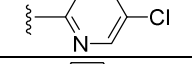
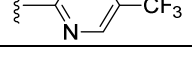
Calculated (Truncated System)			
	$\Delta G$ (kcal/mol)	$\Delta\Delta G$ (kcal/mol)	
<b>10</b>	-20.8	1.3	
<b>11</b>	-22.1	0.0	
Experimental (Full System)			
	$\Delta G$ (kcal/mol)	$\Delta\Delta G$ (kcal/mol)	PDE2A IC <sub>50</sub> (nM) / (LipE)
<b>1</b>	-12.3	1.1	1.6 (5.9)
<b>29</b>	-13.4	0.0	0.3 (6.6)

The observed increase in potency enabled us to pursue analogs of calculated reduced lipophilicity relative to **1** in our search for compounds of low clearance, acceptable human half-life, and reduced estimated human dose (Table 5).

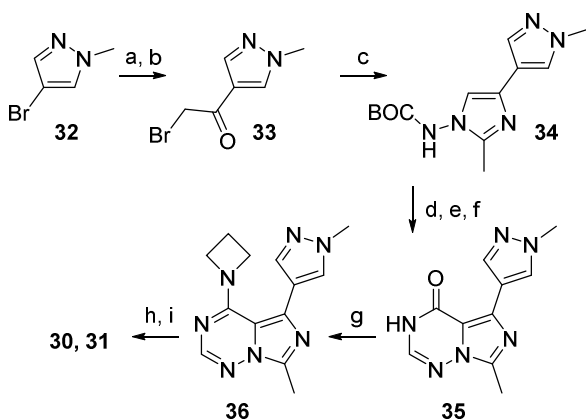
Table 5. Targeted imidazotriazine analogs of potentially lower lipophilicity



Cpd. ID	-NRR	-Ar	cLogP
---------	------	-----	-------

<b>30</b>			1.6
<b>31</b>			1.3
<b>39</b>			3.0
<b>40</b>			1.9

A route similar to that for the synthesis of **29** was developed to access **30** and **31** using a C-H arylation to install the trifluoromethyl and chloropyridine groups (Scheme 2). Thus, 4-bromo-1-methylpyrazole (**32**) was lithiated and trapped with *N*-methoxy-*N*-methylacetamide to afford the methyl ketone which was selectively monobrominated to yield  $\alpha$ -bromoketone **34**. In a manner similar to that depicted in Scheme 1, **34** was converted to **35**. Activation of **35** followed by treatment with azetidine provided **36**. A palladium-catalyzed C-H arylation on the pyrazole C-5 position with heteroaryl halides yielded final targets **30** and **31**. It was found that C-H arylation chemistry was superior to Suzuki coupling for heteroaromatic derivatives, likely due to instability of the required heteroaryl boronates.



Scheme 2. Synthesis of imidazotriazine analogs **30** and **31** using a C-H arylation. (a) *n*-BuLi, *N*-methoxy-*N*-methyl acetamide, THF, -78 °C, 57% (b) pyridinium-Br<sub>3</sub>, EtOH, CH<sub>2</sub>Cl<sub>2</sub>, 23 °C, 89% (c) **24**, DIPEA, 2-MeTHF/DME, reflux, 69% (d) TFA, CH<sub>2</sub>Cl<sub>2</sub>, 23 °C, 92% (e)

1  
2  
3 formamidinium acetate, 2-butanol, 100 °C, 90% (f) CDI, THF, reflux, 70% (g) i. 1H-1,2,4-triazole,  
4  
5 POCl<sub>3</sub>, Et<sub>3</sub>N, CH<sub>3</sub>CN, 70 °C; ii. azetidine-HCl, Et<sub>3</sub>N, 91%. (h) 2-bromo-5-  
6  
7 (trifluoromethyl)pyridine, allylpalladium(II) chloride dimer, K<sub>2</sub>CO<sub>3</sub>, dioxane, reflux, 93% (i) 2-  
8  
9 bromo-5-chloropyridine, allylpalladium(II) chloride dimer, K<sub>2</sub>CO<sub>3</sub>, dioxane, reflux, 52%.

15 The imidazotriazine **30** yielded a 6x PDE2A IC<sub>50</sub> potency increase versus **4** with a similar  
16  
17 MDR BA/AB efflux ratio and slightly higher HLM Cl<sub>int</sub>, resulting in an improved estimated  
18  
19 human dose of 49 mg/day (Table 6). The 5-chloropyridine derivative **31** proved less potent than  
20  
21 **30**, but with a favorable reduction in lipophilicity afforded improved HLM Cl<sub>int</sub> and provided a  
22  
23 lower human dose projection.  
24  
25

26  
27 Table 6. PDE2A Potency, ADME, and Lipophilicity Measures for Imidazotriazine Analogs  
28

	<b>4</b>	<b>30</b>	<b>31</b>	<b>39</b>	<b>40</b>
PDE2A IC <sub>50</sub> (nM)	9	1.6	8.2	1.3	11
HLM Cl <sub>int</sub> (ml/min/kg)	30	52	13	33	9.5
MDR BA/AB	1.5	1.4	1.1	1.2	1.6
Estimated human dose (mg/day)	178	49	45	20	65
SFlogD	--	2.3	1.7	2.8	1.8
LipE	--	6.5	6.4	6.1	6.2

42 HLM Cl<sub>int</sub> = intrinsic clearance apparent scaled determined from human liver microsomes (HLM).  
43  
44 MDR BA/AB = ratio of basolateral-to-apical/apical-to-basolateral flux in Madin-Darby Canine Kidney  
45  
46 (MDCK) cells transfected with the multidrug-resistance gene (MDR1) that encodes for human P-  
47  
48 glycoprotein (P-gp). See Equation 1b for estimated human dose. SFlogD = shake flask logD; LipE = (-  
49  
50 log<sub>10</sub>(PDE2A IC<sub>50</sub>) – SFlogD).  
51

52 In order to understand the clearance pathways to support designing lower clearance analogs,  
53  
54 metabolite identification studies in HLM on **30** were conducted (Figure 7). Results from this *in*  
55  
56  
57  
58  
59  
60

*in vitro* evaluation revealed significant metabolism of the azetidine at both the 2 and 3 positions, yielding the acid **37** and 3-hydroxy azetidine **38**, which were significantly less active than **30** (PDE2A IC<sub>50</sub> = 72 nM and 12 nM, respectively), with both compounds likely to have low brain availability (low passive permeability for **37**, MDCK AB = 1.1 x 10<sup>-6</sup> cm/sec; MDR BA/AB efflux ratio = 12 for **38**). Rat and dog liver microsomes and hepatocytes produced the same metabolites as HLM and human hepatocytes (HHep) suggesting related clearance pathways across species.

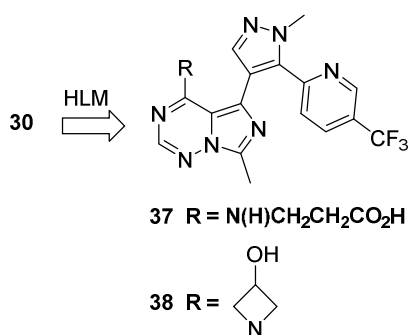
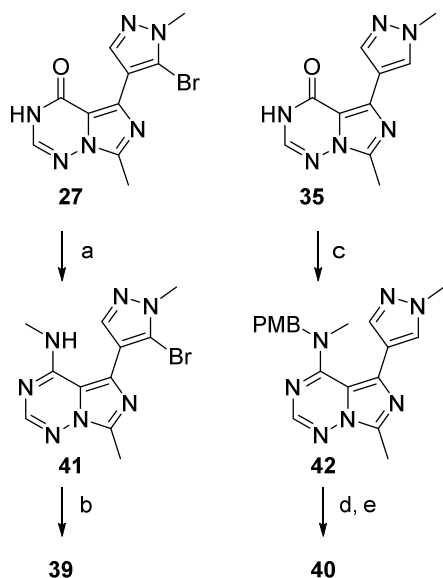


Figure 7. Structures of metabolites of **30** in HLM.

Efforts to simultaneously remove azetidine metabolically reactive sites while reducing lipophilicity led to the preparation of *N*-methyl analogs **39** and **40** via routes related to previous compounds (Scheme 3). Activation of **27** and reaction with methyl amine afforded **41** which was subsequently subjected to a Suzuki cross-coupling with 4-(trifluoromethyl)phenyl boronic acid to yield **39**. In the synthesis of **40**, activation of **35** and S<sub>N</sub>Ar with *N*-methyl-(*p*-methoxybenzyl)amine provided **42**, the *p*-methoxybenzyl (PMB) group being important in facilitating the subsequent C-H arylation with 2-bromo-5-(trifluoromethyl)pyridine. Acidic removal of the PMB proceeded cleanly to yield **40**.



Scheme 3. Synthesis of **39** and **40**. (a) i. 1H-1,2,4-triazole, POCl<sub>3</sub>, Et<sub>3</sub>N, CH<sub>3</sub>CN, 70 °C; ii. MeNH<sub>2</sub>, Cs<sub>2</sub>CO<sub>3</sub>, DMF, 23 °C, 78%. (b) 4-(trifluoromethyl)phenyl boronic acid, Pd(Ph<sub>3</sub>P)<sub>4</sub>, K<sub>3</sub>PO<sub>4</sub>, EtOH, H<sub>2</sub>O, 75% (c) i. 1H-1,2,4-triazole, POCl<sub>3</sub>, Et<sub>3</sub>N, CH<sub>3</sub>CN, 70 °C; ii. MeNH(4-methoxybenzyl), Et<sub>3</sub>N, 23 °C, 76% (d) 2-bromo-5-(trifluoromethyl)pyridine, allylpalladium(II) chloride dimer, K<sub>2</sub>CO<sub>3</sub>, dioxane, reflux, 50% (e) TFA, anisole, CH<sub>2</sub>Cl<sub>2</sub>, reflux, 63%.

The analog **39** demonstrated a combination of potency, moderate microsomal clearance, and low MDR BA/AB efflux to yield the lowest human dose projection (Table 6). The corresponding 5-trifluoromethylpyridine **40** suffered in potency relative to **39** (ca. 10x), but HLM Cl<sub>int</sub> also dropped significantly which contributed to an acceptable estimated human dose.

Overall, these examples highlight the importance of considering both potency and ADME properties for evaluation of compound drug-likeness. Indeed, the LipE for the compounds in Table 6 are all close as a result of the reduced lipophilicity of the lower potency compounds.

In terms of cross-PDE activity, targets **30**, **31**, **39**, and **40** each maintained generally high selectivity over other PDE families in line with previously observed data for the **1** (Table 6).

Table 6. PDE Selectivity for **30**, **31**, **39**, and **40**<sup>a</sup>

Compound	<b>30</b>	<b>31</b>	<b>39</b>	<b>40</b>
<b>PDE2A IC<sub>50</sub> (nM)</b>	1.6	8.2	1.3	11
PDE Selectivity				
PDE1B1	>56250	1556	22945	7808
PDE3A1	>56250	2915	>69231	>8181.8
PDE4D3	>56250	875	>69230	>56250
PDE5A1	>56250	4647	>69230	>8182
PDE6 (Bovine)	>56250	>10976	>69230	>8182
PDE7B	26969	3292	34658	>8182
PDE8B	>56250	>10976	>69231	>8182
PDE9A1	>56250	>10976	>69231	>8182
PDE10A1	2030	372	2370	1049
PDE11A4	50090	3979	>69231	>8182

a) PDE selectivity defined as the ratio of PDEX IC<sub>50</sub> / PDE2A IC<sub>50</sub>. PDE selectivity color legend – red: <1000; orange: 1000-5000; green: >5000.

The four compounds **30**, **31**, **39**, and **40** were next evaluated in a rat oral exploratory toxicity study for up to 15 days, at doses of 5, 50, and 250 mg/kg/day. Despite similarities in structure, there were notable *in vivo* tolerability differences across this dose range and development-limiting microscopic findings in the heart and vasculature were observed with both **31** and **39**. Because of the degenerative nature of the findings and the low exposure margins from both the maximal plasma concentrations ( $C_{max}$ ) and average plasma concentrations ( $C_{av}$ ) of active drug relative to those expected to achieve efficacy (see Supporting Information), these compounds were not advanced.

Compounds **30** and **40**, however, were generally well tolerated at all doses and in particular, there was no evidence of injury in the heart or vasculature which was attributed to either compound in this study, despite high circulating plasma and brain exposures achieved. Comparing off-target pharmacology (Cerep) did not show any significant differences in **30**, **31**, **39**, and **40** that would contribute to the varying toxicity findings. These results are interesting as the small variations in structure from a trifluoromethyl to chloro (**30** to **31**) and

phenyl to pyridyl (**39** to **40**), result in measurable *in vivo* tolerability differences and demonstrate the challenge in predicting *in vivo* drug toxicity.<sup>16</sup>

In a subsequent single dose dog study, **30** was tolerated at doses up to 30 mg/kg, and produced no microscopic findings, including in the heart or vasculature, when administered at doses up to 15 mg/kg/day for 14 days. In contrast, **40** produced the microscopic finding of arteriopathy within the arteries of the heart at high and intermediate doses ( $\geq 20$  mg/kg/day). Exposure margins at the no observable effect level (NOEL), the lowest dose tested, for arteriopathy, were insufficient to continue advancement of **40** into development. During development, **30** was administered to rats and dogs in studies up to 1 month in duration. Target organs identified in these studies included skeletal muscle (rats) and the central nervous system (rats and dogs); no effects were observed in the heart or vasculature. Based upon the lack of development-limiting *in vivo* safety findings with **30**, further *in vitro* and *in vivo* pharmacological and pharmacokinetic profiling was carried out.

The testing of **30** across a panel of kinases and other targets (Cerep) showed minimal activity (see Supporting Information), demonstrating highly selective inhibition of PDE2A. We next evaluated the ability of **30** to displace radiolabeled **2** in rat, dog, and monkey striatal tissue in order to establish binding to native PDE2A which yielded a  $K_i = 4.2 - 8.4$  nM (Table 7). These values are within ca. 3-5 fold of the PDE2A enzyme  $IC_{50}$ .

Table 7.  $K_i$  values for displacement of **2** by **30** in striatal tissue and comparison to PDE2A  $IC_{50}$

Species	$K_i$ (nM)	$K_i /$ PDE2A $IC_{50}$
Rat	4.2	2.6
Dog	8.4	5.2
Monkey	5.5	3.4

We have previously reported that the NMDA antagonist MK-801 can disrupt low frequency cortical delta oscillation in cortical electroencephalogram (EEG) recordings in rat brain, and that PDE2A inhibition with **1** can reverse these deficits.<sup>4</sup> In this model, **30** showed complete reversal of MK-801's effects at 0.1 mg/kg over the experiment time course (data not shown). At 0.03 mg/kg, the reversal of MK-801 was observed at early time points with the effect diminishing over time and thus allowed for effective modeling of *in vivo* potency (Figure 8). Similar activity in terms of both the extent of reversal of the MK-801 effect and the similar fold PDE2A IC<sub>50</sub> C<sub>bu</sub> necessary to achieve the reversal as compared to **1** were achieved (Table 8).

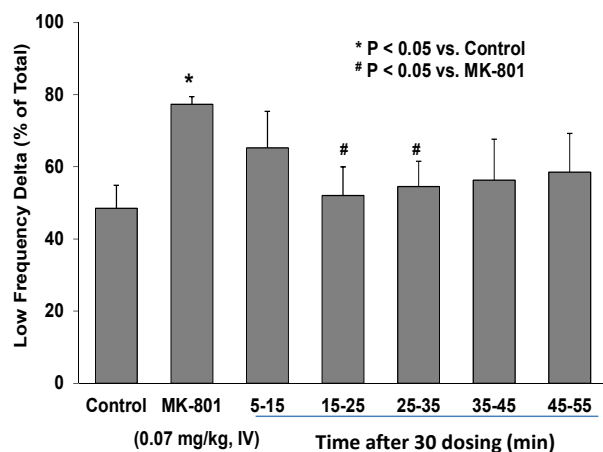


Figure 8. **30** reverses the effect of MK-801 on cortical EEG low frequency delta in rats, 0.03 mg/kg (iv dose). N = 4. Statistical significance was determined by means of two-tailed paired Student's t-tests.

Table 8. Comparison of PDE2A IC<sub>50</sub> and cortical EEG IC<sub>80</sub> C<sub>bu</sub> values

ID	PDE2A IC <sub>50</sub> (nM)	EEG IC <sub>80</sub> (C <sub>bu</sub> , nM)	EEG IC <sub>80</sub> / PDE2A IC <sub>50</sub>
<b>1</b>	1.6	11	7
<b>30</b>	1.6	9	6

EEG = Electroencephalogram.

1  
2  
3 As with **1**,<sup>4</sup> the examination of behavioral effects of **30** revealed no impact upon either  
4 spontaneous or habituated locomotor activity in rats (sc dose range 0.32, 1.0 and 3.2 mg/kg, data  
5 not shown). No effects of **30** (sc dose range 0.32, 1.0, and 3.2 mg/kg) were seen in the  
6 conditioned avoidance responding assay, a measure used to predict antipsychotic potential, and  
7 when dosed in combination with risperidone (0.032 and 0.32 mg/kg) did not alter the efficacy of  
8 risperidone (data not shown). Compound **30** did, however, significantly attenuate the working  
9 memory errors produced by ketamine in a working memory radial arm maze (RAM) model in  
10 rats (0.032 to 0.32 mg/kg, SC dosing, Figure 9), demonstrating an ability to ameliorate deficits  
11 produced by the NMDA antagonist. Satellite pharmacokinetic studies were used to estimate the  
12  $C_{bu}$  levels associated with the efficacious doses, and ranged from 3.1 nM (0.1 mg/kg) to 12.5 nM  
13 (0.32 mg/kg). At a dose of 1 mg/kg, however, the beneficial effect of **30** was significantly  
14 attenuated, leading to a U-shaped dose-response curve. A similar profile was also produced in  
15 this assay in studies using an AMPA positive allosteric modulator.<sup>17</sup> With regard to a potential  
16 mechanistic understanding of this process, recent reports have shown that PDE2A inhibition can  
17 potentiate aspects of dopamine D1 receptor signaling *in vitro*<sup>18</sup> and it is well established that  
18 working memory tasks typically demonstrate peak performance within an optimal range of  
19 dopamine signaling.<sup>19</sup> Thus, it is possible that the U-shaped dose response curve by **30** in the  
20 RAM test could be due to augmented D1 signaling exceeding an optimal range at higher doses,  
21 which would be important to consider in a clinical setting.  
22  
23  
24  
25  
26  
27  
28  
29  
30  
31  
32  
33  
34  
35  
36  
37  
38  
39  
40  
41  
42  
43  
44  
45  
46  
47  
48  
49  
50  
51  
52  
53  
54  
55  
56  
57  
58  
59  
60

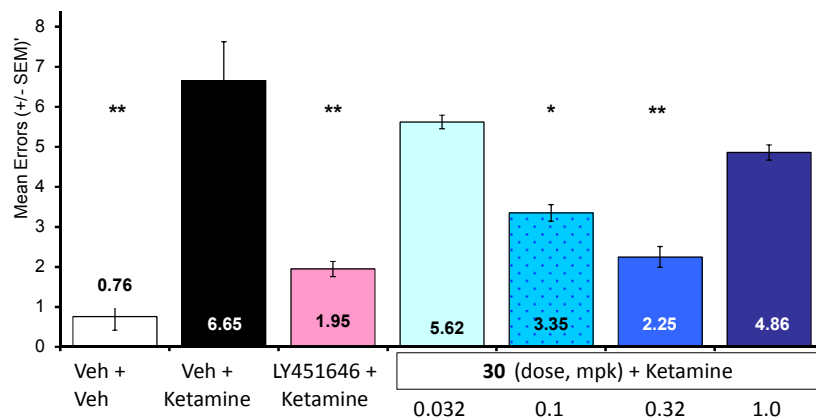


Figure 9. The effect of **30** in a ketamine-disrupted RAM working memory task in rats. N = 20-23. Statistical method – Hochberg where \*, \*\* =  $p < 0.05, 0.01$  vs. Vehicle + ketamine.

Administration of **30** to mice led to an acute and exposure-dependent elevation in the accumulation of bulk levels of cGMP in the cortex, striatum and hippocampus (Figure 10), but no changes in cAMP and the associated downstream phospho-cAMP response element-binding protein (p-CREB) as previously reported for **1**.<sup>4</sup> Given the established activity of PDE2 toward cAMP, this suggests that the specific pool of cAMP regulated by PDE2A in these brain regions may be relatively small relative to the total intracellular pool of cAMP measured in bulk biochemical studies. Measurement of drug exposure in satellite animals was used to model the cGMP response across brain regions. Following the dose response study, a time course study was conducted to evaluate the temporal relationship between  $C_{bu}$  and cGMP response. Upon confirmation of the direct response nature of cGMP levels to  $C_{bu}$  of **30**, results from the dose response study and the time course study were combined in order to estimate the potency of **30**. A linear model best described the relationship between  $C_{bu}$  and the corresponding cGMP increase in all three brain regions using the current dose range and resulted in the estimated potencies across the three brain regions that were quite comparable (Table 9). The  $C_{bu}$   $E_{50}$  values in the mouse brain cGMP assay are significantly higher than the measured EEG  $IC_{80}$  and

RAM  $C_{bu}$  values. A positron emission tomography (PET) study in non-human primates showed 50% PDE2A occupancy by **30** at  $C_{bu} = 57$  nM, also several-fold higher than the EEG  $IC_{80}$  and RAM  $C_{bu}$  values.<sup>20</sup> These results suggest that localized and/or small changes in cGMP may lead to these *in vivo* effects and that low measured levels of target occupancy could be sufficient for human efficacy.

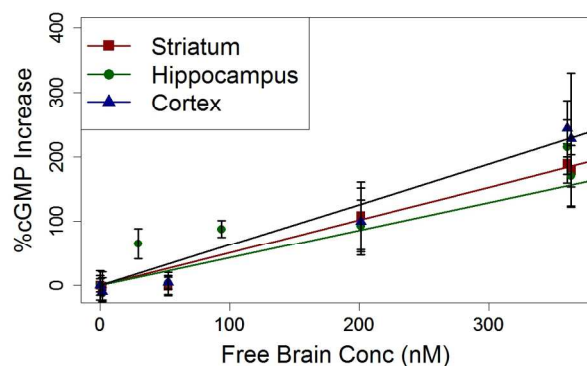


Figure 10. Mouse brain cGMP dose response for **30**

Table 9. Estimated potency for cGMP increase of **30** across different brain regions

Brain region	Striatum	Hippo-campus	Cortex
Slope <sup>a</sup> (%/nM)	0.51	0.43	0.63
$C_{bu}$ $E_{50}$ <sup>b</sup>	98.0	116.3	79.4

a) Slope definition (%/nM): % increase in cGMP per nM of drug free in brain ( $C_{bu}$ ). b) Projected  $C_{bu}$  associated with 50% increase in brain region cGMP levels

A variety of *in vitro* and *in vivo* pharmacokinetic assays were next used to profile **30**. An assessment for potential drug-drug interactions (DDIs) with **30** showed no direct or time-dependent inhibition of metabolism by representative human recombinant cytochrome P450 (CYP) enzymes (1A2, 2B6, 2C8, 2C9, 2C19, 2D6 and 3A) and no induction of CYP1A2. *In vitro*, **30** was identified as a weak inducer of CYP3A4, however the risk of DDIs at the estimated

clinically relevant exposures was predicted to be low. Metabolism of **30** was primarily by CYP3A4 and was expected to have a high risk eliciting DDIs via increased plasma levels of **30** if co-administered with both highly and moderately potent clinically-relevant inhibitors of CYP3A4, such as ketoconazole or erythromycin. This risk is mitigated, however, since the majority of schizophrenia drugs which could be dosed with **30** are not typically CYP3A4 inhibitors and that large pre-clinical safety margins were obtained with **30** from toxicology studies in rats and dogs which could afford modest upward fluctuations in exposure levels upon co-administration.

The  $C_{bu}/C_{pu}$  and cerebrospinal fluid/ $C_{pu}$  ratio ( $(CSF)/C_{pu}$ ) for **30** were evaluated across different species from multiple studies (Table 10, see Supporting Information for full details). In these studies, **30** demonstrated consistent access to brain and CSF, supporting the ability of **30** to readily engage PDE2A in the central nervous system and built confidence in doing the same in humans. These data, along with the high passive permeability in Ralph Russ Canine Kidney (RRCK) cells ( $26 \times 10^{-6}$  cm/s) and low MDR BA/AB efflux ratio, suggest that it is reasonable to use  $C_{bu}/C_{pu} = 1$  in human dose projections based upon a recent analysis.<sup>21</sup>

Table 10. Mean  $C_{bu}/C_{pu}$  and  $CSF/C_{pu}$  of **30** in Mouse, Rat, Dog, and Monkey

Species	$C_{bu}/C_{pu}$	$CSF/C_{pu}$
CD-1 Mouse	0.51 <sup>a</sup>	0.65 <sup>a</sup>
Wistar-Han Rat	0.71 <sup>b</sup>	1.85 <sup>d</sup>
Beagle Dog	0.58 <sup>c</sup>	0.68 <sup>c</sup>
Cynomolgus Monkey	0.60 <sup>a</sup>	0.81 <sup>c</sup>
Overall Average	0.65	0.98

(a) Determined from one study. (b) Average from seven different studies. (c) Average from three different studies. (d) Average from two different studies.  $C_{bu}/C_{pu}$  = unbound brain

concentration/unbound plasma concentration;  $CSF/C_{pu}$  = cerebrospinal fluid/unbound plasma concentration.

Following iv administration in rat, **30** demonstrated a high plasma clearance ( $CL_p$ ) of 122 mL/min/kg, which was not predicted by rat liver microsomes using the well-stirred model (28.3 ml/min/kg). Combined with a moderate steady state volume of distribution ( $V_{ss}$ ) of 3.9 L/kg, **30** had a short half-life ( $t_{1/2}$ ) of 1.4 hours in rat (Table 11). In dog, the  $CL_p$  was low (12.3 mL/min/kg) and was consistent with the prediction from dog liver microsomal clearance ( $CL_p$  <13.4 ml/min/kg) which supported using HLM  $Cl_{int}$  to predict human  $CL_p$ . No metabolism of **30** by aldehyde oxidase was observed and scaled clearance in HHep (HHep  $Cl_{int}$  = 44 ml/min/kg) was similar to that in HLM, suggesting minimal non-CYP mediated metabolism that provided further support in using HLM  $Cl_{int}$  to predict human  $CL_p$ .

Table 11. Mean Pharmacokinetics of **30** in Rat and Dog Following Single Oral and iv Dose Administration

Species	N	Dose (mk/kg)/Route	$C_{max}$ (ng/mL)	$T_{max}$ (h)	$AUC_{inf}$ (ng•h/mL)	$CL_p$ (mL/min/kg)	$V_{ss}$ (L/kg)	$T_{1/2}$ (hour)	%F
Wistar-Han Rat	2	5/Oral <sup>b</sup>	363	0.08	312	--	--	1.4	44
		1/iv <sup>c</sup>	1020 <sup>d</sup>	--	141	122	3.94	1.1	--
Beagle Dog	2	5/Oral <sup>e</sup>	1770	0.25	4120	--	--	4.1	57
		0.3/iv <sup>b</sup>	293 <sup>d</sup>	--	431	12.3	2.89	5.0	--

-- = Not calculated;  $AUC_{inf}$  = Area under the concentration time curve from time 0 to infinity;  $CL_p$  = Plasma clearance;  $C_{max}$  = Maximum observed concentration; % F = Bioavailability; N = number of animals; Oral = Oral gavage;  $t_{1/2}$  = Terminal elimination phase half-life; SBECD = sulfobutylether- $\beta$ -cyclodextrin;  $T_{max}$  = Time of the first occurrence of  $C_{max}$ ;  $V_{ss}$  = Steady-state volume of distribution.

a.  $F (\%) = ([AUC_{inf} (\text{Oral}) \times \text{Dose (IV)}] / [AUC_{inf} (\text{IV}) \times \text{Dose (Oral)}]) \times 100$

b. Vehicle was 20% SBECD + 2 molar equivalent of 1N hydrochloric acid.

- 1  
2  
3 c. Vehicle was 2 molar equivalent of 1N hydrochloric acid.  
4  
5 d. Extrapolated concentration to time zero ( $C_0$ ).  
6  
7 e. Vehicle was 0.5% methylcellulose + 2 molar equivalent of 1N hydrochloric acid  
8  
9

10  
11 The predicted  $CL_p$  of **30** in humans (8.8 ml/min/kg) was estimated using HLM  $Cl_{int}$  in the  
12 well-stirred model, adjusted for human plasma and microsomal protein binding and afforded an  
13 estimated bioavailability of 32% (Table 12). Human predicted  $V_{ss}$  was approximated using the  
14 rat and dog  $V_{ss}$  values adjusted for differences in species plasma protein binding, and yielded a  
15 value of 1.9 L/kg. The estimated human  $t_{1/2}$  was 2.5 h. Using the aforementioned predicted  
16 pharmacokinetic parameters with a  $C_{av,ss}$  of 11 ng/mL,<sup>22</sup> a predicted human dose of 30 mg/day  
17 was estimated, close to the value of 49 mg/day determined from *in vitro* values in Equation 1b.  
18  
19  
20  
21  
22  
23  
24  
25  
26

27 Table 12. Human predictions of **30**: Pharmacokinetics and efficacious dose based upon  
28 animal data.  
29  
30  
31

$Cl_p$ (mL/min/kg)	8.8		F (%)	32
$V_{ss}$ (L/kg)	1.9		$C_{av,ss}$ QD Dose (mg/day)	30
$t_{1/2}$ (h)	2.5			

32  
33  
34  
35  
36  
37  
38  
39  
40  
41  
42  $Cl_p$  = Plasma clearance; F% = Bioavailability;  $F_a$  = Fraction absorbed;  $t_{1/2}$  = half life;  $V_{ss}$  =  
43 Volume of distribution at steady state.  
44  
45  
46

47 To ensure that the mechanism of action is adequately evaluated for efficacy of a drug, it is  
48 often desirable to administer doses that will allow minimum drug concentrations ( $C_{min}$ ) to remain  
49 above an efficacious concentration threshold for the entire dosing interval versus maintaining an  
50 average concentration. Since the data from both the mouse cGMP and rat cortical EEG models  
51 suggested that these effects were the result of direct PDE2A inhibition, we utilized  
52  
53  
54  
55  
56  
57  
58  
59  
60

1  
2  
3 pharmacokinetic modeling using projected PK parameters presented in Table 12 to explore  
4 human doses of **30** that would be projected to maintain  $C_{\min}$  at or above the  $C_{\text{av,ss}}$  target of 11  
5 ng/mL for 24 hrs. The  $C_{\text{av,ss}}$  based 30 mg immediate release (IR) oral dose of **30** was predicted  
6 to maintain exposure at or above the targeted  $C_{\min}$  for approximately 7 h (Figure 11a). A single  
7 dose of 2700 mg IR could sustain the  $C_{\min}$  threshold over 24 h but it was predicted to have a  $C_{\max}$   
8 that was above the human  $C_{\max}$  exposure limit established from the exposure-limiting finding of  
9 convulsions in female rats (Figure 11b). We next modeled 90 mg, twice-daily dosing (BID),  
10 which suggested that sustained plasma levels at or above  $C_{\min}$  were attainable for 24 h with an  
11 acceptable plasma  $C_{\max}$  (Figure 11c). In order to further mitigate against adverse events while  
12 maintaining  $C_{\min}$  exposure and minimizing total drug exposure as based on the area under the  
13 concentration-time curve (AUC), a modified-release (MR) formulation was considered.  
14 Importantly, the ADME and physical properties of **30**, especially permeability and  
15 thermodynamic solubility (340 ug/mL, pH 6.6 buffer), were suitable for development of an MR  
16 formulation with a release duration of approximately 8-10 hours utilizing an osmotic release  
17 mechanism. Subsequent modeling indicated that a 25 mg MR, BID dosing paradigm could  
18 maintain  $C_{\min}$  plasma levels for 24 h (Figure 11d), reducing overall dose almost 4-fold when  
19 compared to the 90 mg IR, BID formulation. It was decided that this MR formulation would be  
20 evaluated in human clinical trials and is the subject of future publications.  
21  
22  
23  
24  
25  
26  
27  
28  
29  
30  
31  
32  
33  
34  
35  
36  
37  
38  
39  
40  
41  
42  
43  
44  
45

---

46 a)

47 b)

---

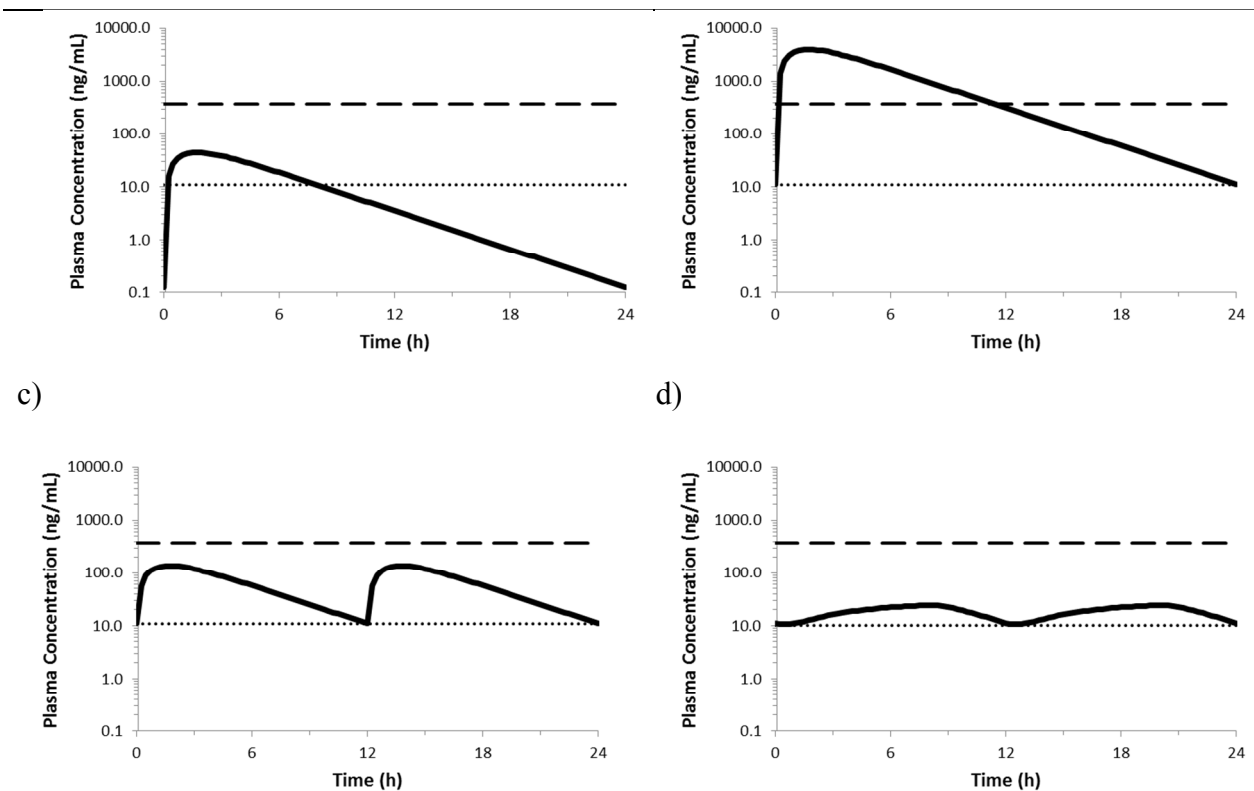


Figure 11. Predicted human plasma concentration profiles of **30** using different oral dosing paradigms and formulations at steady state. a) 30 mg IR, QD. b) 2700 mg IR, QD. c) 90 mg IR, BID. d) 25 mg MR, BID. Dotted lines = 11 ng/mL. Dashed lines = 374 ng/mL (human C<sub>max</sub> exposure limit based on 1/10<sup>th</sup> the convulsion NOEL from 1-month rat toxicology study). BID = twice daily; IR = immediate release; NOEL= no observed effect level; QD = once daily.

### Discussion and Conclusions

Starting with pyrazolopyrimidine lead **1**, potential potency improvement through the use of an imidazotriazine core was identified via application of hydrogen bond acceptor strength calculations. These potency enhancements were realized upon synthesis of target molecules, providing four compounds (**30**, **31**, **39**, **40**) with low projected human dose, high PDE selectivity, and reduced lipophilicity relative to **1**. Multi-day *in vivo* toleration studies of these compounds

1  
2  
3 revealed significant differences in histopathological findings with only small differences in  
4 structure. The superior safety profile of **30** led to further evaluation of its *in vitro* and *in vivo*  
5 PDE2A activity. Radioligand **2** was displaced from brain tissue by **30** with a  $K_i$  ranging from  
6 4.2-8.4 nM, with this higher value being close to the cortical EEG  $IC_{80}$  related  $C_{bu}$  value of 9 nM  
7 and efficacious ketamine RAM  $C_{bu}$  measures of 3.1 to 12.5 nM. In line with the PDE inhibitory  
8 activity of **30**, mouse brain cGMP levels increased with increasing drug exposure in a direct,  
9 linear manner in multiple brain regions. This pharmacology data is comparable to that observed  
10 with **1** and supports the ability of **30** to have potential impact on functional measures disrupted  
11 by NMDA receptor hypofunction, which could include cognitive endpoints impacted in  
12 schizophrenia. Pharmacokinetic analyses across species built confidence in human brain  
13 penetration with  $C_{bu}/C_{pu}$  approaching unity, along with good oral bioavailability, resulting in a  
14 predicted  $C_{av,ss}$ -based dose in human of 30 mg/day. In order to ensure constant inhibition of  
15 PDE2A via a  $C_{min}$  dosing paradigm, pharmacokinetic modeling suggested that a ca. 50 mg/day  
16 (25 mg, BID) MR formulation of **30** could achieve this and an extended release formulation  
17 approach was planned to be explored in human volunteers.  
18  
19  
20  
21  
22  
23  
24  
25  
26  
27  
28  
29  
30  
31  
32  
33  
34  
35  
36  
37  
38  
39

#### 40 *Experimental Section*

##### 41 42 43 Chemistry

44  
45  
46 Experiments were generally carried out under inert atmosphere (nitrogen or argon), particularly  
47 in cases where oxygen- or moisture-sensitive reagents or intermediates were employed.  
48 Commercial solvents and reagents were generally used without further purification, including  
49 anhydrous solvents where appropriate (generally Sure-Seal<sup>TM</sup> products from the Aldrich  
50 Chemical Company, Milwaukee, Wisconsin). Mass spectrometry (MS) data is reported from  
51  
52  
53  
54  
55  
56  
57  
58  
59  
60

1  
2  
3 liquid chromatography-mass spectrometry (LCMS) or atmospheric pressure chemical ionization  
4 (APCI) instrumentation. Chemical shifts for nuclear magnetic resonance (NMR) data are  
5 expressed in parts per million (ppm,  $\delta$ ) referenced to residual peaks from the deuterated solvents  
6 employed, or to tetramethylsilane standard with multiplicities given as s (singlet), br (broad), d  
7 (doublet), t (triplet), dt (doublet of triplets), q (quintet), m (multiplet). Compound purity was  
8 determined by high performance liquid chromatography (HPLC) and all final test compounds  
9 were >95% purity. All final compounds were assessed for purity by HPLC via the following  
10 general conditions: **Column:** Waters Atlantis dC18 4.6x50, 5 $\mu$ ; Mobile phase A: 0.05% TFA in  
11 water (v/v); Mobile phase B: 0.05% TFA in acetonitrile (v/v); **Gradient:** 95.0% water/5.0%  
12 acetonitrile linear to 5% water/95% acetonitrile in 4.0min, HOLD at 5% water/95% acetonitrile  
13 to 5.0min. Flow: 2mL/min.

14  
15  
16  
17  
18  
19  
20  
21  
22  
23  
24  
25  
26  
27  
28  
29 *4-(azetidin-1-yl)-7-methyl-5-(1-methyl-5-(4-(trifluoromethyl)phenyl)-1H-pyrazol-4-*  
30 *yl)imidazo[5,1-f][1,2,4]triazine (29), Scheme 1.*

31  
32  
33  
34  
35  
36  
37  
38  
39  
40  
41  
42  
43  
44  
45  
46  
47  
48  
49  
50  
51  
52  
53  
54  
55  
56  
57  
58  
59  
60  
*Step A. Ethyl 5-bromo-1-methyl-1H-pyrazole-4-carboxylate.* Copper(II) bromide (99%,  
20.0 g, 88.6 mmol) and *tert*-butyl nitrite (90%, 14.1 mL, 107 mmol) were combined in  
acetonitrile (65 mL) and heated to 65 °C. Ethyl 5-amino-1-methyl-1H-pyrazole-4-carboxylate  
(**21**) (10.0 g, 59.1 mmol) was slowly added portion-wise {Caution: gas evolution!} and the  
reaction was maintained at 65 °C for 24 hours. The mixture was cooled to room temperature,  
poured into aqueous hydrochloric acid (3 N, 600 mL), diluted with ethyl acetate (300 mL) and  
stirred for 10 minutes. The aqueous layer was extracted with ethyl acetate (150 mL), and the  
combined organic layers were dried over magnesium sulfate, filtered and concentrated *in vacuo*.  
The residue was purified via silica gel chromatography (sample loaded in minimal  
dichloromethane; Gradient: 5% to 100% ethyl acetate in heptane, with a 5-minute hold at 32%),

1  
2  
3 affording the product as a pale yellow solid. Yield: 9.10 g, 39.0 mmol, 66%. LC/MS  $m/z$  233.3  
4  
5 (M+1).  $^1\text{H}$  NMR (500 MHz,  $\text{CDCl}_3$ )  $\delta$  1.36 (t,  $J=7.1$  Hz, 3H), 3.92 (s, 3H), 4.32 (q,  $J=7.1$  Hz,  
6  
7 2H), 7.93 (s, 1H).  
8  
9

10 *Step B.* 5-bromo-1-methyl-1H-pyrazole-4-carboxylic acid (**22**). A suspension of ethyl 5-  
11  
12 bromo-1-methyl-1H-pyrazole-4-carboxylate (see previous) (8.00 g, 34.3 mmol) in  
13  
14 tetrahydrofuran (60 mL), water (20 mL) and MeOH (20 mL) was treated with lithium hydroxide  
15  
16 monohydrate (3.17 g, 75.5 mmol) and stirred for 4 hours at room temperature. Removal of  
17  
18 solvents under reduced pressure provided a white solid residue, which was diluted with water (50  
19  
20 mL), washed with diethyl ether (50 mL) and adjusted to pH 2.5 with aqueous 6 N hydrochloric  
21  
22 acid. The thick suspension was extracted with 2-methyltetrahydrofuran (2 x 125 mL), and the  
23  
24 combined organic layers were dried over magnesium sulfate, filtered and concentrated *in vacuo*  
25  
26 to provide the product as an off-white solid. Yield: 6.49 g, 31.7 mmol, 92%. LC/MS  $m/z$  205.2  
27  
28 (M+1).  $^1\text{H}$  NMR (500 MHz,  $\text{DMSO}-d_6$ )  $\delta$  3.86 (s, 3H), 7.91 (s, 1H), 12.64 (br s, 1H).  
29  
30  
31  
32

33 *Step C.* 2-bromo-1-(5-bromo-1-methyl-1H-pyrazol-4-yl)ethanone (**23**). A solution of 5-  
34  
35 bromo-1-methyl-1H-pyrazole-4-carboxylic acid (**22**) (6.4 g, 31 mmol) in methanol (100 mL) was  
36  
37 placed in a water bath, treated in a single portion with sodium methoxide (95%, 1.86 g, 32.7  
38  
39 mmol) and stirred for 30 minutes at room temperature. After removal of volatiles *in vacuo*, the  
40  
41 sodium salt was concentrated twice from heptane (100 mL). It was then suspended in  
42  
43 dichloromethane (100 mL) and treated with oxalyl chloride (3.15 mL, 35.9 mmol) followed by  
44  
45 *N,N*-dimethylformamide (2 drops). The reaction was stirred for 20 hours at room temperature,  
46  
47 and then concentrated under reduced pressure. The solid residue was suspended in acetonitrile  
48  
49 (100 mL), treated drop-wise with a solution of (trimethylsilyl)diazomethane in  $\text{Et}_2\text{O}$  (2 M, 39.0  
50  
51 mL, 78.0 mmol) and stirred for 3 hours. The mixture was cooled to 0 °C and hydrogen bromide  
52  
53  
54  
55  
56  
57  
58  
59  
60

1  
2  
3 (33% in acetic acid, 21.9 mL, 125 mmol) was added drop-wise. After 1 hour at 0 °C, the  
4  
5 reaction mixture was concentrated, and the solid residue was mixed with heptane (250 mL) and  
6  
7 reconcentrated. The residue was diluted with ethyl acetate (100 mL), and vigorously stirred with  
8  
9 saturated aqueous sodium bicarbonate solution (100 mL). The organic layer was dried over  
10  
11 magnesium sulfate, filtered and concentrated *in vacuo*; the crude product was purified via silica  
12  
13 gel chromatography (Sample loaded in a minimum quantity of dichloromethane; Gradient: 12%  
14  
15 to 100% ethyl acetate in heptane) to afford the product as an off-white solid, of approximately  
16  
17 85% purity by LCMS analysis. Yield: 8.10 g, approximately 78% (corrected for purity). LC/MS  
18  
19 *m/z* 282.8 (M+1). <sup>1</sup>H NMR (500 MHz, CDCl<sub>3</sub>) δ 3.93 (s, 3H), 4.25 (s, 2H), 8.01 (s, 1H).  
20  
21  
22  
23

24 *tert-butyl 2-ethanimidoylhydrazinecarboxylate (24)*. Sodium hydroxide (16.0 g, 400 mmol)  
25  
26 was dissolved in absolute ethanol (1000 mL) at 60 °C. The solution was cooled to 0 °C and  
27  
28 treated portion-wise with ethyl ethanimidoate hydrochloride (50 g, 400 mmol); after 10 minutes,  
29  
30 *tert-butyl hydrazinecarboxylate* (52.9 g, 400 mmol) was added in a single portion. The reaction  
31  
32 was warmed to 70 °C and was stirred at 70 °C for 2.5 hours. The mixture was then cooled to 20  
33  
34 °C and filtered. The filtrate was concentrated *in vacuo* and treated with *tert-butyl methyl ether*  
35  
36 (500 mL) and ethanol (20 mL). After seeding, the mixture was allowed to stir for 18 hours, after  
37  
38 which time the precipitated solid was collected via filtration and washed with ice-cold *tert-butyl*  
39  
40 *methyl ether* (500 mL). The solid was dissolved in 2-methyltetrahydrofuran : methanol (9:1  
41  
42 mixture, 300 mL), and the solution was concentrated to dryness. The residue was washed with  
43  
44 diethyl ether (3x200 mL) and dried, affording the product as a very pale yellow solid. Yield; 50.  
45  
46 2 g, 290 mmol, 72%. LC/MS *m/z* 174.3 (M+1). <sup>1</sup>H NMR (500 MHz, CD<sub>3</sub>OD) δ 1.47 (s, 9H),  
47  
48 1.88 (s, 3H).  
49  
50  
51  
52  
53  
54  
55  
56  
57  
58  
59  
60

1  
2  
3        *Step D.*        *tert-butyl [4-(5-bromo-1-methyl-1H-pyrazol-4-yl)-2-methyl-1H-imidazol-1-*  
4 *yl]carbamate (25).*    *tert*-Butyl 2-ethanimidoylhydrazinecarboxylate (**24**) (5.9 g, 34 mmol), 2-  
5 bromo-1-(5-bromo-1-methyl-1H-pyrazol-4-yl)ethanone (**23**) (8.00 g, approximately 24 mmol)  
6 and *N,N*-diisopropylethylamine (10.9 mL, 62.6 mmol) were heated to reflux in a mixture of 2-  
7 methyltetrahydrofuran (200 mL) and 1,2-dimethoxyethane (50 mL). After 2.5 hours, the  
8 reaction was cooled and washed with 50% saturated aqueous sodium chloride solution (75 mL).  
9 The aqueous layer was extracted with 2-methyltetrahydrofuran (50 mL), and the combined  
10 organic layers were dried over magnesium sulfate, filtered and concentrated *in vacuo*. The  
11 residue was chromatographed (Gradient: 0% to 8% methanol in dichloromethane), and the  
12 purified material (7.5 g) was dissolved in diethyl ether (25 mL), treated with hexane (4 drops),  
13 and allowed to crystallize. The resulting solid was collected and washed with a small amount of  
14 cold diethyl ether to provide the product as a very pale pink solid. Yield: 6.49 g, 18.2 mmol,  
15 59% over 2 steps. LCMS *m/z* 358.4 (M+1). <sup>1</sup>H NMR (500 MHz, CDCl<sub>3</sub>) δ 1.49 (br s, 9H), 2.16  
16 (br s, 3H), 3.85 (s, 3H), 7.17 (s, 1H), 7.89 (s, 1H), 8.8-9.3 (br s, 1H).  
17  
18  
19  
20  
21  
22  
23  
24  
25  
26  
27  
28  
29  
30  
31  
32  
33

34        *Step E.*        *4-(5-bromo-1-methyl-1H-pyrazol-4-yl)-2-methyl-1H-imidazol-1-amine,*  
35 *trifluoroacetate salt.*    *tert*-Butyl [4-(5-bromo-1-methyl-1H-pyrazol-4-yl)-2-methyl-1H-imidazol-  
36 1-yl]carbamate (**25**) (5.00 g, 14.0 mmol) was dissolved in dichloromethane (120 mL), treated  
37 with trifluoroacetic acid (20.9 mL, 281 mmol), and stirred for 2.5 hours. After removal of  
38 volatiles *in vacuo*, the oily residue was diluted with diethyl ether (100 mL). The resulting  
39 suspension was stirred for 30 minutes at room temperature, and then the solid was collected and  
40 washed with diethyl ether to provide the product as an off-white solid. Yield: 4.98 g, 13.5  
41 mmol, 96%. LCMS *m/z* 256.3 (M+1). <sup>1</sup>H NMR (500 MHz, CD<sub>3</sub>OD) δ 2.65 (s, 3H), 3.95 (s,  
42 3H), 7.68 (s, 1H), 7.86 (s, 1H).  
43  
44  
45  
46  
47  
48  
49  
50  
51  
52  
53  
54  
55  
56  
57  
58  
59  
60

1  
2  
3 *Step F. N-[4-(5-bromo-1-methyl-1H-pyrazol-4-yl)-2-methyl-1H-imidazol-1-yl]imidoformamide*  
4 **(26)**. 4-(5-Bromo-1-methyl-1H-pyrazol-4-yl)-2-methyl-1H-imidazol-1-amine, trifluoroacetate  
5 salt (see previous) (4.90 g, 113.2 mmol) was combined with formamidine acetate (98%, 4.92 g,  
6 46.3 mmol) in 2-butanol (40 mL), and the reaction mixture was heated at 100 °C for 6 hours,  
7 then allowed to cool to room temperature and stir for 18 hours. The off-white solid was  
8 collected by filtration and washed with 2-propanol followed by diethyl ether. The solid was then  
9 triturated with aqueous ammonium hydroxide (7.5 M, 40 mL); filtration provided a white solid,  
10 which was washed with 2-propanol followed by diethyl ether to provide the product. Yield:  
11 2.70 g, 9.54 mmol, 72%. <sup>1</sup>H NMR (500 MHz, CD<sub>3</sub>OD), presumed to be a mixture of rotamers or  
12 tautomers: δ 2.26 and 2.31 (2 s, 3H), 3.89 and 3.89 (2 s, 3H), 7.26 and 7.40 (2 s, 1H), 7.41 and  
13 7.96 (2 br s, 1H), 7.85 and 7.82 (2 s, 1H).

14  
15  
16  
17  
18  
19  
20  
21  
22  
23  
24  
25  
26  
27  
28 *Step G. 5-(5-bromo-1-methyl-1H-pyrazol-4-yl)-7-methylimidazo[5,1-f][1,2,4]triazin-4(3H)-*  
29 *one (27)*. 1,1'-Carbonyldi(1,2,4-triazole) (90%, 2.69 g, 14.8 mmol) and *N*-[4-(5-bromo-1-  
30 methyl-1H-pyrazol-4-yl)-2-methyl-1H-imidazol-1-yl]imidoformamide **(26)** (2.69 g, 9.50 mmol)  
31 were combined in 1,4-dioxane (63 mL) and was stirred for 3.5 hours at room temperature, then  
32 heated to 50 °C for 1 hour. Additional 1,1'-carbonyldi(1,2,4-triazole) (90%, 1.34 g, 7.35 mmol)  
33 was added, and heating was continued for 30 minutes. After another addition of 1,1'-  
34 carbonyldi(1,2,4-triazole) (90%, 269 mg, 1.48 mmol), heating at 50 °C was carried out for an  
35 additional 75 minutes. The reaction was allowed to cool to room temperature, and was then  
36 concentrated to half its original volume; the precipitate was collected and washed with ethyl  
37 acetate to afford a white solid. This was dissolved in methanol (50 mL), concentrated to dryness  
38 and triturated with water (25 mL). After collection of the solid, it was washed with 2-propanol  
39 followed by diethyl ether to provide the product as a white solid. Yield: 1.95 g, 6.31 mmol, 66%.  
40  
41  
42  
43  
44  
45  
46  
47  
48  
49  
50  
51  
52  
53  
54  
55  
56  
57  
58  
59  
60

1  
2  
3 LCMS  $m/z$  309.4 (M+1).  $^1\text{H}$  NMR (500 MHz, DMSO- $d_6$ )  $\delta$  2.53 (s, 3H), 3.87 (s, 3H), 7.87 (s,  
4  
5 1H), 8.17 (s, 1H), 11.69 (br s, 1H).

6  
7 *Step H.* 7-methyl-5-(1-methyl-5-(4-(trifluoromethyl)phenyl)-1H-pyrazol-4-yl)imidazo[5,1-  
8  
9 *ff*[1,2,4]triazin-4(3H)-one (**28**). A mixture of 5-(5-bromo-1-methyl-1H-pyrazol-4-yl)-7-  
10  
11 methylimidazo[5,1-*ff*][1,2,4]triazin-4(3H)-one (**27**) (1 g, 3.235 mmol), 4-(trifluoromethyl)phenyl  
12  
13 boronic acid (799 mg, 4.21 mmol) and  $\text{Cs}_2\text{CO}_3$  (2.64 g, 8.09 mmol) in 2-propanol (30 mL) and  
14  
15  $\text{H}_2\text{O}$  (20 mL) was treated with  $\text{Pd}(\text{dppf})\text{Cl}_2 \cdot \text{CH}_2\text{Cl}_2$  (308 mg, 0.421 mmol) under nitrogen at  
16  
17 room temperature. The solution was then purged with nitrogen for 10 mins followed by heating  
18  
19 to reflux for 3 hours. LC-MS showed the reaction was complete. The mixture was filtered and  
20  
21 the filtrate was concentrated to give the residue which was partitioned between  $\text{H}_2\text{O}$  (50 mL) and  
22  
23 EtOAc (100 mL). The aqueous layer was extracted with EtOAc (3x50 mL). The combined  
24  
25 organic layer was washed with brine (100 mL), dried over  $\text{Na}_2\text{SO}_4$ , filtered and concentrated.  
26  
27 The residue was purified by silica gel chromatography ( $\text{CH}_2\text{Cl}_2$ : MeOH = 100: 1 ~ 10: 1) to give  
28  
29 the product as a light yellow solid. Yield: 700 mg, 18.7 mmol, 58% yield. LC/MS  $m/z$  375.0  
30  
31 (M+1).  $^1\text{H}$  NMR (400 MHz, DMSO- $d_6$ )  $\delta$  8.08 (s, 1H), 7.79 (m, 3H), 7.66 (d,  $J = 8$  Hz, 2H),  
32  
33 3.76 (s, 3H), 2.35 (s, 3H).

34  
35  
36  
37  
38  
39  
40  
41  
42 *Step I.* 4-(azetidin-1-yl)-7-methyl-5-(1-methyl-5-(4-(trifluoromethyl)phenyl)-1H-pyrazol-4-  
43  
44 *yl)imidazo[5,1-*ff*][1,2,4]triazine (29)*. Finely ground 1H-1,2,4-triazole (139 mg, 2 mmol) was  
45  
46 mixed with  $\text{CH}_2\text{Cl}_2$  (2 mL), cooled to 0 °C, and treated drop-wise with phosphorus oxychloride  
47  
48 (50  $\mu\text{L}$ , 0.54 mmol). The suspension was stirred for 1 minute, and then slowly treated drop-wise  
49  
50 with triethylamine (300  $\mu\text{L}$ , 2.14 mmol) under vigorous stirring wherein the mixture changed  
51  
52 from white to pale orange. The mixture was then treated portion-wise with **28** (50 mg, 0.13  
53  
54  
55  
56  
57  
58  
59  
60

1  
2  
3 mmol). At the completion of the addition, the reaction was warmed to room temperature for 4  
4  
5 hrs after which conversion to the triazole intermediate was indicated by TLC (10:1 CH<sub>2</sub>Cl<sub>2</sub> –  
6  
7 MeOH, R<sub>f</sub> = 0.5, bright yellow). The reaction mixture was cooled to 0 °C and was quenched  
8  
9 with water followed by NaHCO<sub>3</sub> (sat. aqueous). The mixture was diluted with EtOAc and the  
10  
11 combined organic layer was washed with water followed by brine, was then dried over sodium  
12  
13 sulfate, filtered, and concentrated. The residue was taken up in DMF (3 mL) and was treated  
14  
15 with azetidine (17.5 uL, 0.26 mmol) and Cs<sub>2</sub>CO<sub>3</sub> (131, 0.39 mmol) at room temperature. After  
16  
17 stirring for 1 h, the reaction was complete by LC/MS. The mixture was diluted with EtOAc and  
18  
19 was washed with water and brine, dried over Na<sub>2</sub>SO<sub>4</sub>, filtered, and concentrated. Purification by  
20  
21 silica gel chromatography (CH<sub>2</sub>Cl<sub>2</sub>-MeOH (0 to 5% gradient) afforded the title compound as a  
22  
23 white solid. Yield: 45.5 mg, 0.11 mmol, 85% yield. LC/MS *m/z* 414.5 (M+1). <sup>1</sup>H NMR (CDCl<sub>3</sub>,  
24  
25 400 MHz) δ 7.79 (s, 1H), 7.64 (s, 1H), 7.62 (d, *J* = 8 Hz, 2H), 7.53 (d, *J* = 8 Hz, 2H), 3.91 (br s,  
26  
27 4H), 2.62 (s, 3H), 2.24 (q, *J* = 8 Hz, 2H), 1.55 (s, 3H).  
28  
29  
30  
31  
32  
33  
34

35  
36 *4-(azetidin-1-yl)-7-methyl-5-(1-methyl-5-(5-(trifluoromethyl)pyridin-2-yl)-1H-pyrazol-4-*  
37  
38 *yl)imidazo[5,1-f][1,2,4]triazine (30) and 4-(azetidin-1-yl)-5-(5-(5-chloropyridin-2-yl)-1-methyl-*  
39  
40 *1H-pyrazol-4-yl)-7-methylimidazo[5,1-f][1,2,4]triazine (31), Scheme 2.*  
41  
42  
43  
44

45 *Step A. 1-(1-methyl-1H-pyrazol-4-yl)ethanone.* 4-Bromo-1-methyl-1H-pyrazole (**32**) (41.3  
46  
47 mL, 400 mmol) was dissolved in tetrahydrofuran (750 mL) and cooled to -78 °C. *n*-Butyllithium  
48  
49 (2.5 M solution in hexanes, 160 mL, 400 mmol) was added drop-wise over 30 minutes, and the  
50  
51 resulting mixture was stirred for 1 hr at -78 °C. After drop-wise addition of a solution of *N*-  
52  
53 methoxy-*N*-methylacetamide (40.9 mL, 400 mmol) in tetrahydrofuran (100 mL) to the -78 °C  
54  
55  
56  
57  
58  
59  
60

1  
2  
3 reaction mixture, the cooling bath was allowed to warm to 0 °C over 4 hrs. The reaction was then  
4  
5 quenched with saturated aqueous sodium chloride solution (50 mL), and volatiles were removed  
6  
7 in vacuo. The residue was diluted with ethyl acetate (1000 mL), treated with magnesium sulfate,  
8  
9 and stirred for 30 minutes before being filtered and concentrated in vacuo. Purification was  
10  
11 carried out via silica gel chromatography (material was loaded in a minimum amount of  
12  
13 dichloromethane; Gradient: 5% to 100% ethyl acetate in heptane) to provide a pale yellow oil  
14  
15 that solidified on standing. Yield: 28.5 g, 230 mmol, 57%. <sup>1</sup>H NMR (500 MHz, CDCl<sub>3</sub>) δ 2.37  
16  
17 (s, 3H), 3.90 (s, 3H), 7.83 (s, 1H), 7.84 (s, 1H).  
18  
19

20  
21 *Step B: 2-bromo-1-(1-methyl-1H-pyrazol-4-yl)ethanone (33).* A solution of 1-(1-methyl-1H-  
22  
23 pyrazol-4-yl)ethanone (see previous) (28.5 g, 230 mmol) in dichloromethane (400 mL) was  
24  
25 diluted with absolute ethanol (100 mL) and treated portionwise with pyridinium tribromide  
26  
27 (95%, 773 g, 230 mmol). The reaction was stirred at room temperature for 3 hours, during  
28  
29 which time it solidified; the mixture was diluted with dichloromethane (300 mL) and water (400  
30  
31 mL), treated with sodium sulfite (5 g) and stirred for 10 minutes. The organic layer was dried  
32  
33 over magnesium sulfate, filtered and concentrated in vacuo. The residue was washed with water  
34  
35 (200 mL), collected by filtration, washed again with water, and dried to afford the product as an  
36  
37 off-white solid. Yield: 41.6 g, 205 mmol, 89%. <sup>1</sup>H NMR (500 MHz, CDCl<sub>3</sub>) δ 7.97-7.98 (m,  
38  
39 1H), 7.95 (br s, 1H), 4.17 (s, 2H), 3.95-3.96 (m, 3H).  
40  
41  
42  
43  
44

45 *Step C. tert-butyl [2-methyl-4-(1-methyl-1H-pyrazol-4-yl)-1H-imidazol-1-yl]carbamate (34)*  
46  
47 *tert*-Butyl 2-ethanimidoylhydrazinecarboxylate (17.3 g, 99.9 mmol), 2-bromo-1-(1-methyl-1H-  
48  
49 pyrazol-4-yl)ethanone (**33**) (16.89 g, 83.18 mmol) and *N,N*-diisopropylethylamine (31.9 mL, 183  
50  
51 mmol) were combined in ice-cold 2-methyltetrahydrofuran (400 mL) and 1,2-dimethoxyethane  
52  
53 (100 mL), and the reaction mixture was heated to reflux. After 2.5 hours, the reaction was  
54  
55  
56  
57  
58  
59  
60

1  
2  
3 cooled and washed with 50% saturated aqueous sodium chloride solution (75 mL). The aqueous  
4 layer was extracted with 2-methyltetrahydrofuran (100 mL), and the combined organic layers  
5 were dried over magnesium sulfate, filtered and concentrated *in vacuo*. The residue was  
6 dissolved in warm ethyl acetate (60 mL), allowed to cool to room temperature, then cooled to 5  
7 °C for 30 minutes. The resulting solid was collected by filtration and washed with a small  
8 quantity of cold ethyl acetate, then washed with diethyl ether, to provide the product as a very  
9 pale yellow solid. Yield: 16.0 g, 57.7 mmol, 69%. LC/MS *m/z* 278.5 (M+1). <sup>1</sup>H NMR (500  
10 MHz, CDCl<sub>3</sub>) δ 1.49 (br s, 9H), 2.23 (s, 3H), 3.84 (s, 3H), 6.87 (s, 1H), 7.51 (s, 1H), 7.60 (s,  
11 1H), 8.67 (br s, 1H).

12  
13  
14  
15  
16  
17  
18  
19  
20  
21  
22  
23  
24 *Step D.* 2-methyl-4-(1-methyl-1*H*-pyrazol-4-yl)-1*H*-imidazol-1-amine, trifluoroacetate salt. A  
25 solution of *tert*-butyl [2-methyl-4-(1-methyl-1*H*-pyrazol-4-yl)-1*H*-imidazol-1-yl]carbamate (**34**)  
26 (8.0 g, 29 mmol) in CH<sub>2</sub>Cl<sub>2</sub> (200 mL) and trifluoroacetic acid (40 mL) was stirred at room  
27 temperature for 2.5 hours. After removal of solvents *in vacuo*, the residue was stirred in 1:1  
28 ethyl acetate/ heptane for 18 hours. The resulting solid was isolated by filtration to provide the  
29 product as a white solid. Yield: 5.3 g, 18 mmol, 62%. The mother liquor was concentrated *in*  
30 *vacuo*, and the residue was stirred for 30 minutes in a 1:1:1 mixture of ethyl acetate/ heptane/  
31 diethyl ether (50 mL); filtration provided additional product as a white solid. Combined yield:  
32 7.8 g, 26.8 mmol, 92%. <sup>1</sup>H NMR (400 MHz, DMSO-*d*<sub>6</sub>) δ 2.54 (s, 3H), 3.89 (s, 3H), 6.55 (br s,  
33 2H), 7.65 (s, 1H), 7.85 (d, *J*=0.7 Hz, 1H), 8.11 (br s, 1H).

34  
35  
36  
37  
38  
39  
40  
41  
42  
43  
44  
45  
46  
47 *Step E.* *N*-[2-methyl-4-(1-methyl-1*H*-pyrazol-4-yl)-1*H*-imidazol-1-yl]imidoforamide. 2-  
48 Methyl-4-(1-methyl-1*H*-pyrazol-4-yl)-1*H*-imidazol-1-amine, trifluoroacetate salt (see Step D  
49 above) (103.0 g, 353.7 mmol) and formamidine acetate (98%, 131 g, 1.23 mol) were combined  
50 in 2-butanol (350 mL). The reaction was heated to 100 °C for 3 hours, at which time it was  
51  
52  
53  
54  
55  
56  
57  
58  
59  
60

1  
2  
3 allowed to cool to room temperature and diluted with a 2:1 mixture of 10 N sodium hydroxide  
4 solution/ saturated aqueous sodium chloride solution (300 mL). After vigorous stirring, the layers  
5 were separated, and the aqueous layer was extracted with 2-butanol (4 x 250 mL). The  
6 combined organic layers were concentrated *in vacuo*, and the resulting solid was slurried with  
7 acetonitrile (550 mL), stirred for 2 h at room temperature and filtered. The collected solids were  
8 washed with dry acetonitrile (3 x 100 mL), and then dried *in vacuo* at 40 °C for 2 hours to  
9 provide the product as an off-white solid. Yield: 61.5 g, 301 mmol, 85%. The mother liquor  
10 was concentrated to dryness, then dissolved in acetonitrile (200 mL) and allowed to stand for 18  
11 hours. The resulting solid was isolated by filtration to provide additional product as an off-white  
12 solid. Combined yield: 64.8 g, 317 mmol, 90%. <sup>1</sup>H NMR (500 MHz, CD<sub>3</sub>OD), presumed to be a  
13 mixture of rotamers or tautomers: δ 2.25 and 2.29 (2 s, 3H), 3.88 and 3.88 (2 s, 3H), 7.03 and  
14 7.19 (2 s, 1H), 7.39 and 7.94 (2 s, 1H), 7.69 and 7.67 (2 s, 1H), 7.77 and 7.75 (2 s, 1H).

15  
16  
17  
18  
19  
20  
21  
22  
23  
24  
25  
26  
27  
28  
29  
30  
31 *Step F.* 7-methyl-5-(1-methyl-1H-pyrazol-4-yl)imidazo[5,1-f][1,2,4]triazin-4(3H)-one (35).  
32  
33 N-[2-Methyl-4-(1-methyl-1H-pyrazol-4-yl)-1H-imidazol-1-yl]imidoforamide (see Step E  
34 above) (58.3 g, 285 mmol) was combined with 1,1'-carbonyldiimidazole (98%, 59.0 g, 357  
35 mmol) in tetrahydrofuran (1140 mL) at 63 °C, and the suspension was stirred for 2.5 hours at 65  
36 °C. The mixture was cooled and concentrated *in vacuo*; the resulting solid was slurried with  
37 methanol (400 mL), warmed to reflux for 20 minutes and cooled to 7 °C. The solid was  
38 collected to provide the product as a pale yellow solid. Yield: 45.9 g, 199 mmol, 70%. LC/MS  
39 *m/z* 231.1 (M+1). <sup>1</sup>H NMR (500 MHz, DMSO-*d*<sub>6</sub>) δ 2.48 (s, 3H), 3.88 (s, 3H), 7.79 (s, 1H), 8.08  
40 (s, 1H), 8.37 (s, 1H), 11.59 (br s, 1H).

41  
42  
43  
44  
45  
46  
47  
48  
49  
50  
51  
52 *Step G.* 4-azetidin-1-yl-7-methyl-5-(1-methyl-1H-pyrazol-4-yl)imidazo[5,1-f][1,2,4]triazine  
53 (36). Finely ground 1H-1,2,4-triazole (278 g, 4.02 mol) was mixed with acetonitrile (700 mL),  
54  
55  
56  
57  
58  
59  
60

1  
2  
3 cooled to 0 °C, and treated drop-wise with phosphorus oxychloride (62.4 mL, 669 mmol) while  
4 maintaining the internal temperature below 15 °C. The suspension was stirred for 10 minutes,  
5  
6 and then slowly treated drop-wise with triethylamine (607 mL, 4.35 mol) under vigorous stirring,  
7  
8 while keeping the internal temperature below 48 °C. The reaction was stirred for 15 minutes as it  
9  
10 cooled to 41 °C, and was then treated portion-wise with 7-methyl-5-(1-methyl-1H-pyrazol-4-  
11  
12 yl)imidazo[5,1-f][1,2,4]triazin-4(3H)-one (**35**) (77.1 g, 335 mmol). At the completion of the  
13  
14 addition, the reaction was warmed to 70 °C for 1 hour, then cooled to room temperature, at which  
15  
16 point thin layer chromatography (Eluant: 10% methanol in ethyl acetate) indicated complete  
17  
18 conversion to the triazole-substituted intermediate. The reaction slurry was treated successively  
19  
20 with triethylamine (279 mL, 2.00 mol) and azetidine hydrochloride (94.0 g, 1.00 mol); over 10  
21  
22 minutes, the internal temperature rose from 18 °C to 38 °C. The mixture was stirred for 1 hour,  
23  
24 cooled to 15-20 °C and filtered. The filter cake was washed with acetonitrile (600 mL), and the  
25  
26 filtrate was concentrated *in vacuo*. The resulting paste was diluted with water (650 mL)  
27  
28 followed by aqueous sodium hydroxide solution (10 N, 450 mL). This slurry was extracted with  
29  
30 dichloromethane (3 x 350 mL), and the combined organic layers were dried over sodium sulfate  
31  
32 and filtered. This filtrate was passed through a plug of silica gel (230-400 mesh, 150 g), eluting  
33  
34 with dichloromethane (1 L) followed by 10% methanol in ethyl acetate (1 L). The combined  
35  
36 eluants were concentrated *in vacuo*, and the residue was washed with *tert*-butyl methyl ether  
37  
38 (350 mL), collected by filtration, and washed with diethyl ether. This solid was dissolved in  
39  
40 water (200 mL) and diluted once more with aqueous sodium hydroxide solution (5 N, 250 mL).  
41  
42 The mixture was extracted with dichloromethane (3 x 250 mL), and the combined organic layers  
43  
44 were dried over sodium sulfate, filtered and concentrated *in vacuo*. The solid was washed with  
45  
46 *tert*-butyl methyl ether (350 mL) and collected by filtration to afford the product as a pale tan  
47  
48  
49  
50  
51  
52  
53  
54  
55  
56  
57  
58  
59  
60

1  
2  
3 solid. Yield: 82.15 g, 305 mmol, 91%. <sup>1</sup>H NMR (500 MHz, CDCl<sub>3</sub>) δ 2.23-2.30 (m, 2H), 2.65  
4 (s, 3H), 3.96 (s, 3H), 3.98-4.07 (m, 4H), 7.61 (br s, 1H), 7.61 (br s, 1H), 7.85 (s, 1H).  
5  
6

7  
8 *Step H. 4-azetidin-1-yl-7-methyl-5-{1-methyl-5-[5-(trifluoromethyl)pyridin-2-yl]-1H-pyrazol-*  
9 *4-yl}imidazo[5,1-f][1,2,4]triazine (30). 36* (10.0 g, 37.1 mmol), 2-bromo-5-  
10 (trifluoromethyl)pyridine (16.8 g, 74.3 mmol) and ground potassium carbonate (15.4 g, 111  
11 mmol) were combined in a reaction flask, purged with nitrogen, and treated with degassed 1,4-  
12 dioxane (600 mL). To this mixture was added allylpalladium(II) chloride dimer (693 mg, 1.86  
13 mmol), and the system was again purged with nitrogen. The reaction was heated to 102 °C for 36  
14 hours, then cooled and concentrated *in vacuo*. The residue was partitioned between ethyl acetate  
15 (400 mL) and aqueous hydrochloric acid solution (1 N, 200 mL). The aqueous phase was  
16 neutralized with solid sodium bicarbonate and extracted with ethyl acetate (4 x 50 mL). The  
17 combined organic layers were washed with 1 N aqueous citric acid, then with saturated aqueous  
18 sodium bicarbonate solution. After treatment with Darco<sup>®</sup> activated carbon, the organic layer  
19 was dried over sodium sulfate, filtered, and concentrated *in vacuo*. The residue was taken up in a  
20 minimal amount of dichloromethane and concentrated under reduced pressure until it became a  
21 thick oil. Diethyl ether (100 mL) was added, and upon stirring of the mixture, a solid began to  
22 precipitate; stirring was continued for 1 hour at room temperature, and then the white solid was  
23 collected by filtration and washed with diethyl ether. Additional product in the mother liquor  
24 was isolated by concentrating the filtrate *in vacuo* and chromatographing the residue on an  
25 alumina column (Eluant: 70% ethyl acetate in heptane). The product from the column was  
26 recrystallized from warm 20% ethyl acetate in heptane to yield additional product as a white  
27 solid. Combined yield: 5.3 g, 12.8 mmol, 35%. This material was combined with the product of  
28 a similar reaction (total 15.5 g, 37.4 mmol), and further purified as follows. The material was  
29  
30  
31  
32  
33  
34  
35  
36  
37  
38  
39  
40  
41  
42  
43  
44  
45  
46  
47  
48  
49  
50  
51  
52  
53  
54  
55  
56  
57  
58  
59  
60

1  
2  
3 dissolved in a mixture of ethyl acetate (100 mL) and 2-methyltetrahydrofuran (150 mL) at room  
4 temperature. SiliaBond® thiol (SiliCycle, 1.35 mmol/g, 15 g) was added, and the mixture was  
5 stirred for 20 hours, then filtered through Celite. The filtrate was treated with Darco® activated  
6 carbon (500 mg) and stirred for 15 minutes before being filtered and concentrated under reduced  
7 pressure. The resulting oil was azeotroped with a 1:1 mixture of heptane and ethyl acetate to  
8 provide an off-white solid, which was mixed with heptane (100 mL) and stirred at room  
9 temperature for 6 hours. Filtration provided the product as a white solid. Yield: 14.4 g, 93%.  
10 LCMS  $m/z$  415.0 (M+1).  $^1\text{H}$  NMR (400 MHz,  $\text{CDCl}_3$ )  $\delta$  2.17-2.26 (m, 2H), 2.70 (s, 3H), 3.3-3.8  
11 (v br m, 2H), 3.8-4.3 (v br m, 2H), 4.18 (s, 3H), 7.63-7.66 (m, 1H), 7.66 (s, 1H), 7.79-7.83 (m,  
12 2H), 8.95-8.96 (m, 1H). Melting point = 160.8 °C.

13  
14  
15  
16  
17  
18  
19  
20  
21  
22  
23  
24  
25  
26 *Step I. 4-(azetidin-1-yl)-5-(5-(5-chloropyridin-2-yl)-1-methyl-1H-pyrazol-4-yl)-7-*  
27 *methylimidazo[5,1-f][1,2,4]triazine (31).* Synthesis of the title product was carried out  
28 according to the procedure for the synthesis of **30** except that 2-bromo-5-chloropyridine was  
29 used in place of 2-bromo-5-(trifluoromethyl)pyridine. In this case, after the citric acid wash, the  
30 organic layer was dried, filtered and concentrated under reduced pressure to provide a pale  
31 yellow solid, which was then recrystallized from methanol. The solid was dissolved in 2-  
32 methyltetrahydrofuran (300 mL), treated with silica gel and stirred for 18 hours. Darco®  
33 activated carbon (2 g) was added, and the mixture was stirred for 30 minutes, at which time it  
34 was filtered through a pad of Celite and concentrated *in vacuo* to provide the product as a white  
35 solid. Yield: 17.6 g, 46.2 mmol, 52%. LC/MS  $m/z$  381.0 (M+1).  $^1\text{H}$  NMR (400 MHz,  $\text{CDCl}_3$ )  $\delta$   
36 2.16-2.25 (m, 2H), 2.69 (s, 3H), 3.3-3.8 (v br m, 2H), 3.8-4.3 (v br m, 2H), 4.12 (s, 3H), 7.40  
37 (dd,  $J=8.5, 0.7$  Hz, 1H), 7.54 (dd,  $J=8.5, 2.5$  Hz, 1H), 7.64 (s, 1H), 7.81(s, 1H), 8.65 (dd,  $J=2.5,$   
38 0.7 Hz, 1H).  
39  
40  
41  
42  
43  
44  
45  
46  
47  
48  
49  
50  
51  
52  
53  
54  
55  
56  
57  
58  
59  
60

1  
2  
3  
4  
5  
6  
7  
8 *N,7-Dimethyl-5-{1-methyl-5-[4-(trifluoromethyl)phenyl]-1H-pyrazol-4-yl}imidazo[5,1-*  
9 *ff][1,2,4]triazin-4-amine (39), Scheme 3.*

10  
11  
12  
13 *Step Ai. 5-(5-bromo-1-methyl-1H-pyrazol-4-yl)-7-methyl-4-(1H-1,2,4-triazol-1-yl)imidazo[5,1-*  
14 *ff][1,2,4]triazine.* 1H-1,2,4-Triazole (4.49 g, 65.0 mmol) was mixed with acetonitrile (40 mL)  
15 and cooled to 0 °C. Phosphorus oxychloride (1.78 mL, 19.4 mmol) was added, followed by  
16 drop-wise addition of triethylamine (10.9 mL, 78.2 mmol). The temperature was maintained at  
17 15-20 °C for 30 minutes after the completion of the addition. At this point, 5-(5-bromo-1-  
18 methyl-1H-pyrazol-4-yl)-7-methylimidazo[5,1-*ff*][1,2,4]triazin-4(3*H*)-one (27) (2.0 g, 6.5 mmol)  
19 was added, and the reaction mixture was allowed to warm to room temperature, and then heated  
20 to 70 °C for 18 hours. The reaction was cooled and poured into a 10 °C solution of potassium  
21 phosphate (97%, 6.56 g, 30.0 mmol) in water (30 mL). After stirring for 5 minutes, the mixture  
22 was treated with solid sodium chloride (5 g) and stirred for an additional 5 minutes. The layers  
23 were separated, and the aqueous layer was extracted twice with ethyl acetate. The combined  
24 organic layers were washed with saturated aqueous sodium chloride solution, dried over sodium  
25 sulfate, and filtered. Removal of solvents *in vacuo* provided the crude product as an orange paste  
26 (2.1 g; contains some triethylamine by <sup>1</sup>H NMR), which was used in the next reaction without  
27 additional purification. <sup>1</sup>H NMR (400 MHz, CDCl<sub>3</sub>), product peaks: δ 2.86 (s, 3H), 3.89 (s, 3H),  
28 7.66 (s, 1H), 7.94 (s, 1H), 8.36 (s, 1H), 8.95 (s, 1H).

29  
30  
31  
32  
33  
34  
35  
36  
37  
38  
39  
40  
41  
42  
43  
44  
45  
46  
47  
48  
49  
50 *Step Aii. 5-(5-bromo-1-methyl-1H-pyrazol-4-yl)-N,7-dimethylimidazo[5,1-ff][1,2,4]triazin-4-*  
51 *amine (41).* Methylamine (4.31 mL of a 2 M solution in tetrahydrofuran, 8.62 mmol) was added  
52 to a mixture of cesium carbonate (9.78 g, 30.0 mmol) and 5-(5-bromo-1-methyl-1H-pyrazol-4-  
53  
54  
55  
56  
57  
58  
59  
60

1  
2  
3 yl)-7-methyl-4-(1*H*-1,2,4-triazol-1-yl)imidazo[5,1-*f*][1,2,4]triazine (see previous) (2.1 g) in *N,N*-  
4 dimethylformamide (12 mL), and the reaction was stirred at room temperature for 1 hour. It was  
5  
6 quenched with a 1:1 mixture of water and saturated aqueous sodium chloride solution, then  
7  
8 extracted with ethyl acetate (2 x 20 mL) and with tetrahydrofuran (10 mL). The combined  
9  
10 organic layers were dried over sodium sulfate, filtered and concentrated *in vacuo* to provide the  
11  
12 product. Yield: 1.65 g, 5.12 mmol, 78% over 2 steps. LCMS *m/z* 322.1 (M+1). <sup>1</sup>H NMR (500  
13  
14 MHz, CDCl<sub>3</sub>) δ 2.70 (s, 3H), 3.10 (d, *J*=4.9 Hz, 3H), 4.00 (s, 3H), 5.46-5.52 (m, 1H), 7.69 (s,  
15  
16 1H), 7.97 (s, 1H).

17  
18  
19  
20  
21  
22 *Step B. N,7-dimethyl-5-{1-methyl-5-[4-(trifluoromethyl)phenyl]-1*H*-pyrazol-4-yl}imidazo[5,1-*  
23  
24 *f*][1,2,4]triazin-4-amine (39). 5-(5-Bromo-1-methyl-1*H*-pyrazol-4-yl)-*N,7*-dimethylimidazo[5,1-  
25  
26 *f*][1,2,4]triazin-4-amine (41) (13.26 g, 41.16 mmol) and [4-(trifluoromethyl)phenyl]boronic acid  
27  
28 (98%, 9.72 g, 50.2 mmol) were combined in ethanol (126 mL), and the resulting slurry was  
29  
30 treated with a solution of potassium phosphate (98%, 11.13 g, 51.39 mmol) in water (42 mL) and  
31  
32 warmed to 70 °C over 40 minutes while a vigorous nitrogen flow was applied through a bubbler.  
33  
34 After addition of tetrakis(triphenylphosphine)palladium(0) (482 mg, 0.417 mmol), the reaction  
35  
36 mixture was heated at reflux for 3.5 hours, then cooled to room temperature and stirred for an  
37  
38 additional 16 hours. The mixture was filtered through a plug of cotton, and the filtrate was  
39  
40 concentrated *in vacuo*, then reconcentrated with 2-methyltetrahydrofuran (2 x 200 mL). The  
41  
42 residue was reconstituted in 2-methyltetrahydrofuran (150 mL) and extracted with aqueous  
43  
44 hydrochloric acid (1 M, 70 mL, stirred for 20 minutes). The aqueous layer (pH ~2-3) was  
45  
46 discarded. The organic layer was extracted twice with 1 M aqueous hydrochloric acid: first with  
47  
48 100 mL (stirring for 40 minutes), then with 75 mL (stirring for 20 minutes). The 100 mL  
49  
50 aqueous layer was back-extracted with 2-methyltetrahydrofuran (80 mL, stirred for 30 minutes)  
51  
52  
53  
54  
55  
56  
57  
58  
59  
60

1  
2  
3 to remove some color. The two hydrochloric acid layers were combined and treated with  
4  
5 aqueous sodium hydroxide solution (5 M, 35.5 mL), which adjusted the pH to 6. The resulting  
6  
7 mixture was extracted with 2-methyltetrahydrofuran (130 mL); the organic layer was passed  
8  
9 through a plug of sodium sulfate (74 g) and concentrated *in vacuo* to a volume of roughly 150  
10  
11 mL. This was treated with Darco<sup>®</sup> G-60 activated carbon (5.03 g), and spun on a rotary  
12  
13 evaporator in a 50 °C water bath for 1 hour. The warm solution was filtered through a pad of  
14  
15 Celite, rinsing with 2-methyltetrahydrofuran, and the filtrate was concentrated under reduced  
16  
17 pressure. The resulting pale yellow foam was treated with *tert*-butyl methyl ether (150 mL) and  
18  
19 swirled in a 50 °C water bath for 5 minutes, then was cooled to room temperature with stirring  
20  
21 over 1 hour. The resulting slurry was cooled in an ice bath and held for an additional 30  
22  
23 minutes. The solids were collected by filtration and rinsed with chilled (ice – saturated aqueous  
24  
25 sodium chloride solution bath) *tert*-butyl methyl ether (79 mL), then slurried in heptane (150  
26  
27 mL). This mixture was concentrated *in vacuo* to a low volume and reconcentrated with heptane  
28  
29 (2 x 150 mL), to a final volume of approximately 50 mL. Filtration provided the product as a  
30  
31 white solid. Yield: 11.91 g, 30.75 mmol, 75%. LC/MS *m/z* 388.2 (M+1). <sup>1</sup>H NMR (400 MHz,  
32  
33 CDCl<sub>3</sub>) δ 2.65 (br s, 3H), 3.00 (d, *J*=5.0 Hz, 3H), 3.95 (s, 3H), 5.49-5.57 (m, 1H), 7.61 (br AB  
34  
35 quartet, *J*<sub>AB</sub>=8.2 Hz, Δ*v*<sub>AB</sub>=41.4 Hz, 4H), 7.73 (s, 1H), 7.91 (br s, 1H).  
36  
37  
38  
39  
40  
41  
42  
43  
44  
45  
46

47 *N*,7-dimethyl-5-(1-methyl-5-(5-(trifluoromethyl)pyridin-2-yl)-1H-pyrazol-4-yl)imidazo[5,1-  
48  
49 *f*][1,2,4]triazin-4-amine (**40**), Scheme 3.  
50  
51  
52  
53  
54  
55  
56  
57  
58  
59  
60

1  
2  
3        *Step C.*        *N*-(4-methoxybenzyl)-*N*,7-dimethyl-5-(1-methyl-1*H*-pyrazol-4-yl)imidazo[5,1-  
4 *f*][1,2,4]triazin-4-amine (**42**). The product was synthesized in a manner similar to that described  
5  
6 for the preparation of 4-azetidin-1-yl-7-methyl-5-(1-methyl-1*H*-pyrazol-4-yl)imidazo[5,1-  
7 *f*][1,2,4]triazine (**36**), except that 1-(4-methoxybenzyl)-*N*-methylamine was utilized in place of  
8 azetidine hydrochloride, and the workup was modified somewhat: after the slurry was extracted  
9 with dichloromethane, the combined organic layers were washed with 1 N aqueous sodium  
10 hydroxide solution, washed with saturated aqueous sodium chloride solution, and dried over  
11 sodium sulfate. After filtration, the filtrate was concentrated *in vacuo* and passed through a short  
12 column of silica gel (Eluant: 5% methanol in ethyl acetate). The eluant was concentrated under  
13 reduced pressure, and the resulting solid was washed with *tert*-butyl methyl ether followed by  
14 diethyl ether, to provide the product. Yield: 36.0 g, 99.1 mmol, 76%. LC/MS *m/z* 364.2 (M+1).  
15  
16 <sup>1</sup>H NMR (400 MHz, CDCl<sub>3</sub>) δ 2.67 (s, 3H), 2.84 (s, 3H), 3.77 (s, 3H), 3.88 (s, 3H), 4.66 (s, 2H),  
17 6.82 (br d, *J*=8.7 Hz, 2H), 7.07 (br d, *J*=8.6 Hz, 2H), 7.58 (s, 1H), 7.62 (s, 1H), 7.89 (s, 1H).  
18  
19  
20  
21  
22  
23  
24  
25  
26  
27  
28  
29  
30  
31  
32

33        *Step D.*        *Synthesis of N*-(4-methoxybenzyl)-*N*,7-dimethyl-5-{1-methyl-5-[5-  
34 (trifluoromethyl)pyridin-2-yl]-1*H*-pyrazol-4-yl}imidazo[5,1-*f*][1,2,4]triazin-4-amine.        *N*-(4-  
35 Methoxybenzyl)-*N*,7-dimethyl-5-(1-methyl-1*H*-pyrazol-4-yl)imidazo[5,1-*f*][1,2,4]triazin-4-  
36 amine (**42**) (10.0 g, 27.5 mmol), 2-bromo-5-(trifluoromethyl)pyridine (12.4 g, 54.9 mmol) and  
37 powdered potassium carbonate (11.4 g, 82.5 mmol) were combined in 1,4-dioxane (90 mL) and  
38 heated at reflux for 10 minutes. Allylpalladium(II) chloride dimer (98%, 514 mg, 1.38 mmol)  
39 was added, and the reaction was heated for 22 hours at 160 °C in a sealed tube capped with a Q-  
40 Tube™ (Q Labtech). The reaction was cooled to room temperature and concentrated *in vacuo*.  
41 The residue was suspended in ethyl acetate, filtered through Celite and concentrated under  
42 reduced pressure. Silica gel chromatography (Gradient: 50% to 100% ethyl acetate in heptane)  
43  
44  
45  
46  
47  
48  
49  
50  
51  
52  
53  
54  
55  
56  
57  
58  
59  
60

1  
2  
3 provided a pale brown foam (7.85 g), which was crystallized from heptane (~100 mL) and ethyl  
4 acetate (~5 mL) to provide the product as a pale brown powder. Yield: 7.00 g, 13.8 mmol, 50%.  
5  
6 LCMS  $m/z$  509.1 (M+1).  $^1\text{H}$  NMR (500 MHz,  $\text{CDCl}_3$ )  $\delta$  2.54 (s, 3H), 2.72 (s, 3H), 3.75 (s, 3H),  
7  
8 4.14 (s, 3H), 4.34 (br s, 2H), 6.76 (br d,  $J=8.8$  Hz, 2H), 6.94 (br d,  $J=8.5$  Hz, 2H), 7.39 (d,  $J=8.3$   
9  
10 Hz, 1H), 7.72 (s, 1H), 7.76 (dd,  $J=8.3, 2.2$  Hz, 1H), 7.85 (s, 1H), 8.95-8.96 (m, 1H).  
11  
12  
13

14  
15 *Step E.* *N,7-dimethyl-5-{1-methyl-5-[5-(trifluoromethyl)pyridin-2-yl]-1H-pyrazol-4-*  
16  
17 *yl}imidazo[5,1-f][1,2,4]triazin-4-amine (40).* *N*-(4-Methoxybenzyl)-*N,7*-dimethyl-5-{1-methyl-  
18  
19 5-[5-(trifluoromethyl)pyridin-2-yl]-1H-pyrazol-4-yl}imidazo[5,1-f][1,2,4]triazin-4-amine (see  
20  
21 previous) (7.00 g, 13.8 mmol) was dissolved in dichloromethane (46 mL) and treated with  
22  
23 trifluoroacetic acid (40 mL, 520 mmol) and methoxybenzene (99.7%, 7.0 mL, 64 mmol). The  
24  
25 reaction mixture was heated at 40 °C for 4 hours, and then concentrated *in vacuo*. Aqueous 1 N  
26  
27 sodium hydroxide solution was added, and the mixture was extracted with ethyl acetate. The  
28  
29 organic layer was concentrated under reduced pressure to provide crude product (12 g), which  
30  
31 was combined with the crude product from two additional runs of this reaction (total starting  
32  
33 material: 18.09 g, 35.57 mmol). The combined material was dissolved in hot methanol, allowed  
34  
35 to cool slightly, and treated with Darco<sup>®</sup> activated carbon (8 g); this mixture was heated for 1  
36  
37 hour at 50 °C and filtered through Celite. The volume of the filtrate was reduced, and the  
38  
39 solution was left to crystallize for 18 hours. The resulting beige crystals were determined by  $^1\text{H}$   
40  
41 NMR to contain residual methoxybenzene. Trituration with diethyl ether provided the product as  
42  
43 a white solid. Combined yield: 8.73 g, 22.5 mmol, 63%. LCMS  $m/z$  389.2 (M+1).  $^1\text{H}$  NMR (400  
44  
45 MHz,  $\text{CD}_3\text{OD}$ )  $\delta$  2.58 (s, 3H), 2.85 (s, 3H), 4.15 (s, 3H), 7.38 (br d,  $J=8.3$  Hz, 1H), 7.73 (s, 1H),  
46  
47 7.85 (s, 1H), 7.98-8.01 (m, 1H), 9.02-9.04 (m, 1H).  
48  
49  
50  
51  
52  
53  
54  
55  
56  
57  
58  
59  
60

1  
2  
3 *In Vivo Experiments.* All *in vivo* studies were conducted in accordance with the US Animal  
4 Welfare Act and the National Research Council Guide for the Care and Use of Laboratory  
5 Animals. The procedures used in these experiments were approved by an Institutional Animal  
6 Care and Use Committee prior to study conduct.  
7  
8  
9  
10  
11  
12  
13

#### 14 *PDE2-A3 Scintillation Proximity Assay*

15  
16  
17  
18 Human PDE2A isoform sequences to be used for cloning were derived from NCBI accession  
19 entry NR\_026572 for hPDE2A3, respectively. PDE2A isoform sequences were cloned into a  
20 pFastBac1 vector such that an amino terminal FLAG extension and appropriate protease  
21 cleavage sites would be available for subsequent purification steps. Full-length PDE2A3  
22 enzyme was obtained from FLAG purification of sf21 insect cells using standard affinity  
23 purification procedures for this tag (anti-FLAG M2, Sigma Aldrich) or by crude lysate methods.  
24  
25  
26  
27  
28  
29  
30  
31

#### 32 *PDE2-A3 Assay Methodology*

33  
34  
35  
36 Test compounds were solubilized in 100% DMSO and diluted to the required concentrations in  
37 15% DMSO/distilled H<sub>2</sub>O at 5x final concentrations. Compounds were tested at 8  
38 concentrations ranging from 0.316 μM to 0.0001 μM in triplicate. The activity of the test  
39 substances on human PDE2A3 was determined using the [3H]cGMP scintillation proximity  
40 assay format using 384 well plates. The PDE scintillation proximity assay (SPA) yttrium silicate  
41 beads (Perkin Elmer RPNQ0024) preferentially bind the linear nucleotide, GMP, compared to  
42 the cyclic nucleotide, cGMP. Using 3H-cGMP (Perkin Elmer NET337001MC) as the substrate  
43 in this reaction allows the product, 3H-GMP, to be detected using a Wallac Microbeta  
44 scintillation counter. The enzyme concentration for each isoform was determined by enzyme  
45  
46  
47  
48  
49  
50  
51  
52  
53  
54  
55  
56  
57  
58  
59  
60

1  
2  
3 titration experiments to be in the linear range of the assay. The Michaelis constant ( $K_m$ ) of the  
4 enzyme was determined to be 12.8  $\mu\text{M}$  for cGMP. The final substrate concentration used was at  
5 sub- $K_m$  levels so that  $\text{IC}_{50}$  values would approximate the  $K_i$  values. The reaction time was  
6 chosen with respect to the amount of time where 10-20% of substrate was hydrolyzed by the  
7 enzyme. The assay was validated using literature compounds as controls before testing the  
8 representative compounds of the present invention. The corresponding  $\text{IC}_{50}$  values of the  
9 compounds for the inhibition of PDE activities are determined from the concentration-effect  
10 curves by means of non-linear regression.  
11  
12  
13  
14  
15  
16  
17  
18  
19  
20  
21

### 22 *Phosphodiesterase Selectivity Assays*

23  
24 The phosphodiesterase (PDE) assays measure the conversion of 3', 5'-[ $^3\text{H}$ ] cAMP to 5'-[ $^3\text{H}$ ]  
25 AMP (for PDE 1B1, 3A1, 4D3, 7B, 8B and 10A1) or 3', 5'-[ $^3\text{H}$ ] cGMP to 5'-[ $^3\text{H}$ ] GMP (for  
26 PDE 5A1, 6 (Bovine), 9A1 and 11A4) by the relevant PDE enzyme subtype. Yttrium silicate  
27 (YSi) scintillation proximity (SPA) beads bind selectively to 5'-[ $^3\text{H}$ ] AMP or 5'-[ $^3\text{H}$ ] GMP, with  
28 the magnitude of radioactive counts being directly related to PDE enzymatic activity. The assay  
29 was performed in white walled opaque bottom 384-well plates. 1  $\mu\text{l}$  of compound in DMSO was  
30 added to each well. Enzyme solution was then added to each well in buffer (in mM: Trizma, 50  
31 (pH7.5);  $\text{MgCl}_2$ , 1.3 mM) containing Brij 35 (0.01% (v/v)). For PDE1B1 the assay buffer  
32 additionally included  $\text{CaCl}_2$  (30 mM) and calmodulin (25 U/ml). Subsequently, 20  $\mu\text{l}$  of 3',5'-  
33 [ $^3\text{H}$ ] cGMP (125 nM) or 20  $\mu\text{L}$  of 3',5'-[ $^3\text{H}$ ] cAMP (50 nM) was added to each well to start the  
34 reaction and the plate was incubated for 30 min at 25°C. The reaction was terminated by the  
35 addition of 20  $\mu\text{l}$  of PDE YSi SPA beads (Perkin Elmer). Following an additional 8 hour  
36 incubation period the plates were read on a MicroBeta radioactive plate counter (Perkin Elmer)  
37 to determine radioactive counts per well.  
38  
39  
40  
41  
42  
43  
44  
45  
46  
47  
48  
49  
50  
51  
52  
53  
54  
55  
56  
57  
58  
59  
60

### *Data Analysis for In Vitro Studies*

Inhibition curves were plotted from individual experiments, and IC<sub>50</sub> values were determined using a four parameter logistic fit. IC<sub>50</sub> is defined as the concentration of the test article that produced a 50% inhibition of a maximal response. All PDE selectivity data is in the Supporting Information.

*Metabolite Identification Studies in Liver Microsomes or Hepatocytes.* Rat, dog, and/or human microsomes or hepatocytes were obtained from Corning (Prague, Czech Republic) and kept frozen at -80°C until they were thawed at room temperature prior to incubation. Incubation was conducted at Pfizer Inc. (Groton, CT). The final microsomal or hepatocyte P450 concentrations varied from 0.35 to 0.5 μM and were incubated with **30** spiked at 1, 10 or 50 μM with 100 mM phosphate buffer and 1 mM nicotinamide adenine dinucleotide phosphate (NADP) regenerating systems. Mixtures were incubated at 37°C for 1 hour. Following the incubation, samples were quenched with 4x volumes of acetonitrile and spun at 3400 rpm, where the supernatant was evaporated using a Zymark Turbovap (Boston, MA) system at 25°C. The residual sample was reconstituted with 5% aqueous acetonitrile (4 mL) and injected onto either an Agilent Zorbax RXC8 column (Santa Clara, CA) or a Phenomenex, Synergi Fusion RP column (Torrence, CA). LC-MS/MS analysis was carried out using a high performance liquid chromatography system consisting of HP1100 pumps (Hewlett Packard, Palo Alto, CA) with a CTC PAL autosampler (Leap Technologies, Carrboro, NC) interfaced to an LTQ03 (Thermo Scientific, Waltham, MA) ion-trap mass spectrometer and β-RAM ultraviolet (UV) detector. The β-RAM was configured to allow the high performance liquid chromatography (HPLC) effluent from the column to be split with 50 μL introduced to the mass spectrometer and the remaining sample introduced to the UV detector. The mobile phase consisted of solvent A (5 mM ammonium formate) and solvent B

1  
2  
3 (100 % acetonitrile). The gradient was as follows: solvent B was held at 25% for 25 minutes and  
4  
5 ramped from 25% to 70% in 5 minutes, held at 70% for 3 minutes, and then stepped to 25% over  
6  
7 7 minutes. The mass spectrometer was operated using positive electrospray ionization. All raw  
8  
9 data were processed using Analyst Software ver. 1.4.2 (AB Sciex Inc., Ontario, Canada).  
10  
11

12  
13 *Neuropharmacokinetic Studies in CD-1 Mouse, Wistar-Hannover or Sprague-Dawley Rat,*  
14  
15 *Beagle Dog, and Cynomolgus Monkey.*  
16  
17

18 The in-life portion of these studies were conducted at either Pfizer Inc. (Groton, CT, USA) or  
19  
20 Bioduro Inc. (Shanghai, China) while the bioanalytical portions of these studies were conducted  
21  
22 at Pfizer Inc. (Groton, CT). Doses of **30** were administered to mice (SC), rats (intravenously, IV  
23  
24 and/or SC), dogs (orally, PO), and monkeys (SC) prepared as a solution in 20% SBE-BCD  
25  
26 +2ME 1N HCl in a volume of 1 mL/kg for the SC doses, as a solution in 5/5/90,  
27  
28 DMSO/Cremaphor/saline or hydroxypropyl-beta-cyclodextrin acidified for the IV doses, and as  
29  
30 a suspension or solution in acidified 0.5% methylcellulose for the PO doses. Blood samples (for  
31  
32 plasma) were collected via cardiac puncture in ethylenediaminetetraacetic acid (EDTA) treated  
33  
34 tubes at designated times between 2 min and 24 hours while whole brain and/or cerebrospinal  
35  
36 fluid (CSF) samples were collected at the same time points as blood via terminal matrix  
37  
38 samplings. Plasma was isolated after centrifugation and placed on wet ice, while CSF was  
39  
40 collected into tubes via puncture of the cisterna magna and immediately placed on dry ice, and  
41  
42 brains were rinsed with saline and blotted dry before being placed on dry ice. Thawed whole  
43  
44 brain samples were homogenized on ice with water and/or saline 4X the weight as the brain (1:4,  
45  
46 w/v). All samples were stored at  $-80\text{ }^{\circ}\text{C}$  prior to analysis.  
47  
48  
49  
50  
51

52 *Measurement of In Vitro Plasma and Brain Fractions Unbound*  
53  
54  
55  
56  
57  
58  
59  
60

1  
2  
3 The *in vitro* unbound fractions of **30** were determined in mouse, rat, dog, monkey and human  
4 plasma, and in mouse, rat, dog and monkey brain tissue homogenate using a 96-well equilibrium  
5 dialysis method described by Kalvass et al., with the following exceptions at Pfizer Inc. (Groton,  
6 CT). Plasma samples were obtained from BioReclamation (Chestertown, MD) and kept frozen  
7 until they were thawed and pH was adjusted to ~7.4 prior to dialysis. Plasma from the various  
8 species was spiked with 2  $\mu\text{M}$  of **30** and each matrix was dialyzed against an equal volume (150  
9  $\mu\text{L}$ ) of phosphate buffer at 37  $^{\circ}\text{C}$  for 6 h. Following the incubations, equal volumes (50  $\mu\text{L}$ ) of  
10 plasma and buffer samples were collected and mixed with 50  $\mu\text{L}$  of buffer or control plasma,  
11 respectively, for preparation of separate mixed matrix samples. Following the incubations, 15  $\mu\text{L}$   
12 of plasma or 45  $\mu\text{L}$  of buffer samples were collected and mixed with 15 or 45  $\mu\text{L}$  of buffer or  
13 control plasma, respectively, for preparation of mixed matrix samples. All samples were then  
14 precipitated with internal standard in MeCN (200  $\mu\text{L}$ ), vortexed, and centrifuged. Supernatants  
15 were analyzed using an LC–MS/MS assay.  
16  
17  
18  
19  
20  
21  
22  
23  
24  
25  
26  
27  
28  
29  
30  
31  
32

33 Brain homogenates were prepared from freshly harvested mouse, rat, dog, and monkey brains  
34 following dilution with a 4-fold volume of phosphate buffer and spiked with 2  $\mu\text{M}$  (mouse), 2  
35  $\mu\text{M}$  (rat), and 10  $\mu\text{M}$  (dog and monkey) of **30**. The homogenate was dialyzed against an equal  
36 volume (150  $\mu\text{L}$ ) of phosphate buffer at 37  $^{\circ}\text{C}$  for 6 h. Following the incubation, equal volumes  
37 (50  $\mu\text{L}$ ) of brain homogenate and buffer samples were collected and mixed with 50  $\mu\text{L}$  of buffer  
38 or control homogenate, respectively, for preparation of mixed matrix samples. All samples were  
39 then precipitated with internal standard in MeCN (200  $\mu\text{L}$ ), vortexed, and centrifuged.  
40 Supernatants were analyzed using an LC–MS/MS assay. A dilution factor of 5 was applied to  
41 the calculation of brain fraction unbound.  
42  
43  
44  
45  
46  
47  
48  
49  
50  
51  
52  
53  
54  
55  
56  
57  
58  
59  
60

### *Measurement of In Vitro Microsomal Fraction Unbound*

The *in vitro* unbound fraction of **30** was determined in human liver microsomes using pooled microsome samples obtained from Gentest (Prague, Czech Republic), kept frozen at -80°C until they were thawed at room temperature prior to incubation. The final microsomal P450 concentration was 0.25 μM incubated with **30** spiked at 1 μM, 100 mM phosphate buffer, 1 mM nicotinamide adenine dinucleotide phosphate (NADP)-regenerating system using 5 nM isocitric acid and 1 U/mL isocitric dehydrogenase. Mixtures were incubated at 37 °C for 6 h. Following the incubation, equal volumes (50 μL) of microsomes and buffer samples were collected and mixed with 50 μL of buffer or control microsomes respectively, for preparation of mixed matrix samples. All samples were then precipitated with internal standard in acetonitrile (200 μL), vortexed, and centrifuged. Supernatants were analyzed using an LC– MS/MS assay.

### *Pharmacokinetic Studies in Male Wistar Han Rats and Beagle Dogs.*

The in-life and bioanalytical portions of these studies were conducted at Pfizer Inc. (Groton, CT). Male Wistar-Han rats received either a single 1 mg/kg intravenous (IV) dose or a 1 mg/kg oral dose of **30** while dogs received a single 0.3 mg/kg IV dose or a 1 mg/kg oral dose. In both rats and dogs, the IV dose was prepared as a solution in 20% (w/v) sulfobutyl ether β-cyclodextrin with 2M of hydrochloric acid in a volume of 1 mL/kg for rats and 0.4 mL/kg for dogs while the PO doses were prepared as a solution in 0.5% carboxy-methyl cellulose with 1M of hydrochloric acid in a volume of 5 mL/kg in both species. Blood samples were collected in K2EDTA or K3EDTA treated tubes in rats and dogs, respectively at designated times between 2 min and 24 h via carotid artery cannulation. Plasma was isolated after centrifugation and stored at -80 °C prior to analysis.

1  
2  
3     *Generic Liquid Chromatography Tandem Mass Spectrometry (LC–MS/MS) Assay for*  
4  
5     *Exposure Measurements in Plasma, CSF, and/or Brain Homogenate in Various Species.*  
6

7  
8     Plasma, CSF, and/or brain were collected as described above and frozen at  $-80\text{ }^{\circ}\text{C}$  until  
9  
10    analysis by LC –MS/MS. Standard curves were prepared in respective matrices via serial  
11  
12    dilution or mixed matrix (CSF) at various concentration ranges in plasma from 1 to 2000 ng/mL  
13  
14    (mouse), 0.61 to 625 ng/mL (rat), 0.61 to 1250 ng/mL (dog), and 0.61 to 2500 ng/mL (monkey);  
15  
16    in CSF from 0.5 to 1000 ng/mL (mouse), 19.5 to 2500 ng/mL (rat), 0.61 to 1250 (dog), and 0.61  
17  
18    to 2500 ng/mL (monkey); and in brain homogenate from 0.1 to 1000 ng/mL (mouse), 24.4 to  
19  
20    12500 ng/mL (rat), 0.61 to 2500 ng/mL (dog), and 0.61 to 1250 ng/mL (monkey). For plasma,  
21  
22    CSF, or brain homogenate, either a 30  $\mu\text{L}$  (mouse and rat) or 50  $\mu\text{L}$  (dog and monkey) aliquot of  
23  
24    sample was precipitated with 300  $\mu\text{L}$  or 500  $\mu\text{L}$  of acetonitrile containing an internal standard.  
25  
26    Samples were vortexed for 2 minutes and then centrifuged at 3500 rpm for 7 minutes. 150  $\mu\text{L}$  of  
27  
28    the supernatant was transferred to a 96-well plate where 5  $\mu\text{L}$  was injected onto a MacMod  
29  
30    HALO C18 column (Chads Ford, PA). Frozen brain tissue was weighed and a 2-propanol:water  
31  
32    (60:40) volume equivalent to 4 times the mass was added before homogenization in a bead  
33  
34    beater (BioSpec Products Inc., Bartlesville, OK). Brain samples were then extracted in a similar  
35  
36    manner as plasma, mentioned above. CSF samples were assayed using a mixed matrix method  
37  
38    where control plasma and CSF sample (1:1) were mixed prior to extraction using a method  
39  
40    similar to the one described above for plasma. LC–MS/MS analysis was carried out using a high  
41  
42    performance liquid chromatography system consisting of Shimadzu LC20AD pumps (Shimadzu  
43  
44    Scientific Instruments, Columbia, MD) with a CTC PAL autosampler (Leap Technologies,  
45  
46    Carrboro, NC) interfaced to an API 4000 LC–MS/MS quadrupole tandem mass spectrometer  
47  
48    (AB Sciex Inc., Ontario, Canada). The mobile phase consisted of solvent A (5 mM ammonium  
49  
50  
51  
52  
53  
54  
55  
56  
57  
58  
59  
60

1  
2  
3 formate with 0.1% formic acid) and solvent B (100 % acetonitrile). The gradient was as follows:  
4  
5 solvent B was held at 5% for 0.3 min, linearly ramped from 5% to 80% in 1.6 min, held at 80%  
6  
7 for 0.3 min, and then stepped to 5% over 0.01 min. The mass spectrometer was operated using  
8  
9 positive electrospray ionization. All raw data were processed using Analyst Software ver. 1.4.2  
10  
11 (AB Sciex Inc., Ontario, Canada).  
12  
13

### 14 15 16 17 *PDE2A Brain Tissue Binding Assay*

18  
19 Binding assays on membranes from dissected striata from rat, dog and monkey were  
20  
21 performed according to standard procedures. To determine basic assay parameters, ligand  
22  
23 concentrations were determined from saturation binding studies where the K<sub>d</sub> for **2** was found to  
24  
25 be 2.85 nM for rat, 3.18 nM for dog and 3.16 nM for monkey. From tissue concentration curve  
26  
27 studies the optimal amount of tissue was determined to be 1.5 mg/mL for rat and 2.5 mg/mL for  
28  
29 dog and monkey tissue per 96 well plate using 1.5 nM of **2**. These ligand and tissue  
30  
31 concentrations were used in time course studies to determine linearity and equilibrium conditions  
32  
33 for binding. In all species, binding was at equilibrium with the specified amount tissue in 30  
34  
35 minutes. From these parameters, K<sub>i</sub> values were determined by homogenizing the specified  
36  
37 amount of tissue for each species in 50 mM Tris (pH 7.4 at 4 °C) containing 2.0 mM MgCl<sub>2</sub> using  
38  
39 a Polytron and spun in a centrifuge at 40,000 x g for 10 minutes. The pellet was resuspended in  
40  
41 assay buffer (50 mM Tris (pH 7.5) containing 1.3 mM MgCl<sub>2</sub>. Incubations were initiated by the  
42  
43 addition of tissue to 96-well plates containing test drugs and 1.5 nM **2** in a final volume of 250  
44  
45 μL. Non-specific binding was determined by radioligand binding in the presence of a saturating  
46  
47 concentration of BAY-60-7550 (10 μM), a specific PDE2 inhibitor. After 30 minute incubation  
48  
49 period at room temperature, assay samples were rapidly filtered through Unifilter-96 GF/B PEI-  
50  
51  
52  
53  
54  
55  
56  
57  
58  
59  
60

1  
2  
3 coated filter plates and rinsed with ice-cold 50 mM Tris buffer (pH 7.4 at 4 °C). Membrane  
4  
5 bound **2** levels were determined by liquid scintillation counting of the filterplates in  
6  
7 Ecolume. The IC<sub>50</sub> value (concentration at which 50% inhibition of specific binding occurs) was  
8  
9 calculated by linear regression of the concentration-response data in Microsoft Excel. K<sub>i</sub> values  
10  
11 were calculated according to the Cheng-Prusoff equation.  
12  
13

#### 14 *Brain cGMP measures*

15  
16  
17  
18 Brain tissue measurements of cGMP accumulation following drug administration were carried  
19  
20 out as previously described.<sup>23</sup> CD-1 mice were euthanized by focused microwave irradiation of  
21  
22 the brain. Regions of interest were isolated and homogenized in 0.5 N HCL followed by  
23  
24 centrifugation. Supernatant concentrations of cyclic nucleotides were measured using enzyme  
25  
26 immunoassay kits (Cayman Chemical, Ann Arbor, MI). Data were analyzed using a one-way  
27  
28 ANOVA followed by Fishers' PLSD test with the criterion for significance set at p < 0.05.  
29  
30  
31

#### 32 *Electrophysiology assay: Cortical Delta Oscillation*

#### 33 *Animals and surgical procedures*

34  
35  
36  
37 Male Sprague–Dawley rats (Harlan, USA; weighing 250–320 g) under urethane anesthesia @  
38  
39 1.5 g/kg intraperitoneal (IP), were placed in a stereotaxic frame, where craniotomies were  
40  
41 performed above the region of the medial prefrontal cortex (mPFC) and ipsilateral  
42  
43 (CA)1/subiculum. Body temperature of the rat was maintained at 37°C with an electrical heating  
44  
45 pad (Harvard Apparatus, USA). The femoral vein was cannulated for administration of test  
46  
47 drugs. After the conclusion of the experiments animals were euthanized with an IV bolus of  
48  
49 urethane.  
50  
51

#### 52 *Electrophysiological Recordings*

1  
2  
3 Unilateral hippocampal EEG was recorded by a metal, monopolar macro electrode (Rhodes  
4 Medical Instruments, Inc., Model SNEX-300) placed in the mPFC region (co-ordinates: 3.4 mm  
5 anterior from the bregma, 0.6 mm lateral from the midline and 5.0 mm ventral) as described  
6 previously (Kiss et al, 2011). Field potentials were amplified, filtered (0.1-100 Hz), displayed  
7 and digitized at 2000 Hz for on-line and off-line analysis (Spike2 program; Cambridge  
8 Electronic Design, Cambridge, UK). Electrically evoked responses distinguished in the EEG  
9 and quantitative EEG analysis was performed by means of waveform averages and Fast Fourier  
10 Transformation, respectively (Spike2 program). The EEG activity in normal rats under urethane  
11 anesthesia during baseline activity is a synchronous, sinusoidal oscillation which ranges from  
12 1.8 to 2.4 cycles per second (Hz). Following MK-801 administration, the cortical EEG shifts  
13 within the delta band to a less synchronous, higher amplitude signal of 0.5-1.8 Hz. Disruption of  
14 the cortical EEG following MK-801 injection was quantified by calculating the percentage of  
15 total power that occurred in the 0.5-1.8 Hz frequency range compared to the entire 0-4 Hz Delta  
16 band.  
17  
18  
19  
20  
21  
22  
23  
24  
25  
26  
27  
28  
29  
30  
31  
32  
33  
34  
35

### 36 *Behavioral Assays*

37  
38 Male Long Evans rats from Charles River Laboratories (Kingston, NY) ranged between 200-225  
39 g upon arrival and between 400-450 g during the study. Animals were individually housed in  
40 environmentally-controlled quarters (light/dark – 0600 h/1800 h) for one week prior to initiation  
41 of experiments.  
42  
43  
44  
45  
46

### 47 *Spontaneous Locomotor activity*

48  
49 Locomotor activity was measured in 48 custom-made automated activity chambers (30 cm x 30  
50 cm) housed in sound-attenuating cabinets and equipped with photocells and a metal touchplate.  
51  
52  
53  
54 A single 15 watt bulb in each cabinet was controlled by a 24 hour timer which allows the  
55  
56  
57  
58  
59  
60

1  
2  
3 behavioral chambers to be maintained on a 0400 h/1600 h light/dark cycle. Horizontal activity  
4 was measured as crossovers from one quadrant of the cage floor to another, while vertical  
5 locomotor activity (ie rears) was measured as the number of times an animal stood up on its hind  
6 legs against the walls of the chamber, making contact with the metal touch plate. Data were  
7 recorded, stored, and analyzed by a computer equipped with LabView software.  
8  
9

### 14 *Radial Arm Maze*

15  
16  
17 Animals were food-restricted (25-30 g rodent chow/day) beginning 7 days prior to the first day of  
18 exposure to the maze. The eight arm radial maze (Pathfinder Maze System, Lafayette Instrument  
19 Co., Lafayette, IN) contained a food cup at the end of each arm, the contents of which were not  
20 visible from the central platform. The task required that the animals enter each arm to retrieve  
21 the food pellets and use spatial cues in the room in order to remember which arms of the maze  
22 they have previously entered. Permanent visual cues existed within each test room.  
23  
24  
25

26 During training, one reinforcement pellet was placed in the food cup at the end of each arm.  
27  
28

29  
30  
31 Animals were placed on the maze facing away from the experimenter, facing the same arm at the  
32 start of each trial. The timer was started and each arm entry was recorded in sequence. An entry  
33 was defined as all four paws entering an arm of the maze. The animal was allowed to choose  
34 arms until all eight arms were entered and pellets were consumed, until 30 choices were made, or  
35 until 5 min had elapsed, which ever event occurred first. Entry into an arm previously chosen  
36 was counted as an error. If an animal failed to choose all eight arms in 5 min, the arms not  
37 chosen were also counted as errors. Animals were trained once a day on five days per week  
38 (Monday-Friday) and the training criterion was defined as 2 or fewer errors on 2 consecutive  
39 training days.  
40  
41  
42  
43  
44  
45  
46  
47  
48  
49  
50  
51  
52  
53  
54  
55  
56  
57  
58  
59  
60

1  
2  
3 Maze Testing: Once the training criterion was met by all subjects (approximately 15 days of  
4 training), drug testing was initiated. On Mondays and Thursdays all animals were tested to  
5 identify those qualified for compound testing on Tuesdays and Fridays. No testing was  
6 performed on Wednesdays. Animals which committed two or fewer errors on qualifying days  
7 were randomly assigned to treatment groups and were subjected to drug testing by an  
8 experimenter who was blinded as to each animal's treatment. After each qualifying day, animals  
9 to be tested were again randomly assigned to treatment groups and were tested the following  
10 day. This procedure was repeated until the number for each group equaled at least 10, which  
11 typically took between 3 and 4 test days.  
12  
13  
14  
15  
16  
17  
18  
19  
20  
21  
22  
23  
24  
25

### 26 *Computational methods*

27  
28 Hydrogen bond interaction strengths were computed using the Hydrogen Bond workflow in  
29 Jaguar (version 9.0, Schrodinger, LLC, New York, NY 2015) and were extrapolated to the basis  
30 set limit from calculations based on optimization of individual components and complexes at the  
31 LMP2/cc-pVTZ(-f)//X3LYP/6-31G\*\* and LMP2/cc-pVQZ(-g)//X3LYP/6-31G\*\* levels of  
32 theory, including corrections for basis set superposition error. Initial complexes for the PDE5  
33 calculations were derived from the X-ray crystal structures 1XP0 and 1TBF following use of the  
34 Protein Preparation Wizard in Maestro (version 10.4, Schrödinger, LLC, New York, NY, 2015)  
35 by maintaining the ligand positions and deleting the entire protein except for Gln817, the  
36 bridging water to Gln775, or the bridging water to Tyr612. Only the amino acid sidechains  
37 originating from the C $\alpha$  atom were used in the calculations. The initial PDE2 complexes were  
38 generated in an analogous fashion using X-ray crystal structure PDB 5U7L, directly overlaying  
39  
40  
41  
42  
43  
44  
45  
46  
47  
48  
49  
50  
51  
52  
53  
54  
55  
56  
57  
58  
59  
60

1  
2  
3 the bicyclic cores of interest onto the pyrazolopyrimidine core, and deleting the entire protein  
4 except for Gln859, Gln812 and the bridging water to Tyr655.  
5  
6  
7

### 8 *Pharmacokinetic Modeling*

9  
10 The projected pharmacokinetic parameters outlined in Table 12 were used to simulate the  
11 predicted steady-state plasma concentration-time profiles of **30**. A one-compartment open model  
12 with first-order absorption and first-order elimination was used in the simulations (NONMEM  
13 version 7.3; ICON PLC). An 8-hour duration of release was assumed for the MR formulation  
14  
15  
16  
17  
18  
19  
20 simulations.  
21

### 22 *SFLogD assay*

23  
24 The SFlogD assay is a miniaturized octanol/buffer shake flask method used to determine a test  
25 compound's logD value at pH 7.4  
26  
27  
28

29 2 ul of 10 mM test compound in DMSO is added to 149 ul of buffer-saturated 1-octanol.  
30 Following the addition of 149 ul of 1-octanol saturated phosphate buffer, the mixture is  
31 vigorously mixed for 1h at room temperature and subsequently centrifuged at 1000 x g for  
32  
33  
34  
35  
36 15min. Compound concentration from the octanol and buffer phase is determined by LC-MS.  
37

$$38 \log D = \log(\text{Concentration}_{\text{octanol}} / \text{Concentration}_{\text{buffer}})$$

39  
40  
41 1-Octanol saturated phosphate buffer: 20 ml of 1-octanol is added to 2 L of 0.1 M sodium  
42 phosphate buffer, pH 7.4 and vigorously shaken and left standing overnight at room temperature  
43 before using. Buffer-saturated 1-octanol: 20 ml of 0.1M sodium phosphate buffer pH 7.4 is  
44 added to 2 L of 1-octanol and vigorously shaken and left standing overnight at room temperature  
45 before using.  
46  
47  
48  
49  
50  
51

52 *Supporting Information:* PDE2A IC<sub>50</sub> data, number of replicates (n), calculated standard error;  
53 Cerep data for **30**; Kinase selectivity data for **30**; PDE2A brain tissue binding data for **30**;  
54  
55  
56  
57  
58  
59  
60

1  
2  
3 Synthetic route to metabolites **37** and **38**; *In vivo* toleration data table for **30**, **31**, **39**, and **40**;  
4  
5 Comparison of hydrogen bonding strengths between **5** and **6** with PDE5A versus PDE5A IC<sub>50</sub>  
6  
7 measurements; DDI Assay Details; molecular formula strings.  
8  
9

10 *Corresponding Author Information*  
11

12  
13 Christopher J. Helal, [chris.j.helal@pfizer.com](mailto:chris.j.helal@pfizer.com)  
14  
15

16 *Present/Current Author Addresses*  
17

18  
19 Mihaly Hajos: [mihaly.hajos@yale.edu](mailto:mihaly.hajos@yale.edu), Dept. of Comparative Medicine, Yale School of  
20  
21 Medicine, 310 Cedar St., BML 330, P.O. Box 208016, New Haven CT 06520-8016  
22  
23

24 William E. Hoffman: [wehoffma@gmail.com](mailto:wehoffma@gmail.com) 10520 SE 42nd CT, Belleview FL, 34420, (353)  
25  
26 347-5464  
27

28 Zhijun Kang: [zkang@mdanderson.org](mailto:zkang@mdanderson.org) IACS, 3SCR3, MD Anderson, 1881 East Road,  
29  
30 Houston, TX 77054, 713-792-8558  
31  
32

33 Robin J. Kleiman: [robin.kleiman@biogen.com](mailto:robin.kleiman@biogen.com) Biogen, 225 Binney Street, Cambridge, MA  
34  
35 02142 (617) 914 3016  
36  
37

38 Jiemin Lu: [lujamie402@yahoo.com](mailto:lujamie402@yahoo.com) 2623 Misty Grove Dr, Manvel, Texas 77578  
39

40 Noha Maklad: [nmaklad@shire.com](mailto:nmaklad@shire.com) 300 Shire Way, Lexington, MA 02421 (781) 482-1651  
41

42 Laura McDowell: [laura.mcdowell@novartis.com](mailto:laura.mcdowell@novartis.com) Emeryville Campus, 5300 Chiron Way,  
43  
44 Emeryville, CA 94608-2916 (510) 879-9568  
45  
46

47 Dina McGinnis: [casademcginnis@yahoo.com](mailto:casademcginnis@yahoo.com) Mars Pet Care, 2611 Sherrie Ln., Thompson's  
48  
49 Station, TN 37179  
50

51 Patricia A. Seymour: [PASconsult@cox.net](mailto:PASconsult@cox.net) 29 Littlebrook Rd., Westerly, RI 02891 (401)-  
52  
53 742-3696  
54  
55  
56  
57  
58  
59  
60

1  
2  
3 Hirokazu Ueno: [hirokazu\\_ueno@ajinomoto.com](mailto:hirokazu_ueno@ajinomoto.com), Coordination & Management Group, R&D  
4  
5 Planning Dept., AJINOMOTO CO., INC., 15-1 Kyobashi, Tokyo, JAPAN, 104-8315., TEL :  
6  
7  
8 +81-3-5250-8134  
9

10  
11 *Acknowledgments:* We would like to thank Dan Morton, DVM, Ph.D., (deceased) for his  
12  
13 contributions to the *in vivo* toxicology study design and analysis, Victor Guanowsky for running  
14  
15 the rodent locomotor assays, and Douglas Chapin for running the rat CAR assay.  
16

17  
18 *Abbreviations Used:* C<sub>bu</sub>, brain unbound concentration; C<sub>pu</sub>, unbound plasma concentration; CSF,  
19  
20 cerebrospinal fluid; EEG, electroencephalogram; Fa, fraction absorbed; HLM Cl<sub>int</sub>, human liver  
21  
22 microsome intrinsic clearance apparent (ml/min/kg); IR, immediate release; kD, dissociation  
23  
24 constant; LipE, lipophilic ligand efficiency = logIC<sub>50</sub> – SFlogD; MDR BA/AB, ratio of  
25  
26 basolateral-to-apical/apical-to-basolateral flux in cells overexpressing the multi-drug resistant 1  
27  
28 transporter; MR, modified release; PDE2A, phosphodiesterase 2A; RAM, radial arm maze;  
29  
30 SFlogD, shake flask logD; V<sub>ss</sub>, volume of distribution at steady state;  
31  
32

### 33 *References*

34  
35  
36 1. Stephenson, D. T.; Coskran, T. M.; Wilhelms, M. B.; Adamowicz, W. O.; O'Donnell, M.  
37  
38 M.; Muravnick, K. B.; Menniti, F. S.; Kleiman, R. J.; Morton, D. Immunohistochemical  
39  
40 Localization of Phosphodiesterase 2A in Multiple Mammalian Species. *J. Histochem. Cytochem.*  
41  
42 **2009**, *57*, 933-949.  
43  
44

45  
46 2. Boess, F. G.; Hendrix, M.; van der Staay, F.-J.; Erb, C.; Schreiber, R.; van Staveren, W.; de  
47  
48 Vente, J.; Prickaerts, J.; Blokland, A.; Koenig, G. Inhibition of Phosphodiesterase 2 Increases  
49  
50 Neuronal cGMP, Synaptic Plasticity and Memory Performance. *Neuropharmacology* **2004**, *47*,  
51  
52 1081-1092.  
53  
54  
55  
56  
57  
58  
59  
60

1  
2  
3 3. Masood, A.; Huang, Y.; Hajjhussein, H.; Xiao, L.; Li, H.; Wang, W.; Hamza, A.; Zhan, C.-  
4  
5 G.; O'Donnell, J. M. Anxiolytic Effects of Phosphodiesterase-2 Inhibitors Associated with  
6  
7 Increased cGMP Signaling. *J. Pharmacol. Exp. Ther.* **2009**, *331*, 690-699.

8  
9  
10 4. Helal, C. J.; Arnold, E. P.; Boyden, T. L.; Chang, C.; Chappie, T. A.; Fennell, K. F.;  
11  
12 Forman, M. D.; Hajos, M.; Harms, J. F.; Hoffman, W. E.; Humphrey, J. M.; Kang, Z.; Kleiman,  
13  
14 R. J.; Kormos, B. L.; Lee, C.-W.; Lu, J.; Maklad, N.; McDowell, L.; Mente, S.; O'Connor, R. E.;  
15  
16 Pandit, J.; Piotrowski, M.; Schmidt, A. W.; Schmidt, C. J.; Ueno, H.; Verhoest, P. R.; Yang, E.  
17  
18 X. Application of Structure-Based Design and Parallel Chemistry to Identify a Potent, Selective,  
19  
20 and Brain Penetrant Phosphodiesterase 2A Inhibitor. *J. Med. Chem.* **2017**, *60*, 5673-5698.

21  
22 5. For the first x-ray crystal structure of a PDE2A inhibitor inducing a unique pocket see: Zhu,  
23  
24 J.; Yang, Q.; Dai, D.; Huang, Q., X-ray Crystal Structure of Phosphodiesterase 2 in Complex  
25  
26 with a Highly Selective, Nanomolar Inhibitor Reveals a Binding-Induced Pocket Important for  
27  
28 Selectivity. *J Am Chem Soc* **2013**, *135*, 11708-11711.

29  
30 6. For recent disclosures of additional brain penetrant PDE2A inhibitors, see: (a) Mikami, S.;  
31  
32 Nakamura, S.; Ashizawa, T.; Nomura, I.; Kawasaki, M.; Sasaki, S, Oki, H.; Kokubo, H.;  
33  
34 Hoffman, I. D.; Zou, H.; Uchiyama, N.; Nakashima, K.; Kamiguchi, N.; Imada, H.; Suzuki, N.;  
35  
36 Iwashita, H.; Taniguchi, T. Discovery of Clinical Candidate N-((1S)-1-(3-Fluoro-4-  
37  
38 (trifluoromethoxy)phenyl)-2-methoxyethyl)-7-methoxy-2-oxo-2,3-dihydropyrido[2,3-  
39  
40 b]pyrazine-4(1H)-carboxamide (TAK-915): A Highly Potent, Selective, and Brain-Penetrating  
41  
42 Phosphodiesterase 2A Inhibitor for the Treatment of Cognitive Disorders. *J. Med. Chem.* **2017**,  
43  
44 *60*, 7677-7702. (b) Maehara, S.; Arakawa, K.; Hoshida, K.; Nagasue, H.; Chida, N.; Nakao, K;  
45  
46 Furusako, S. Pharmacological Characterization of a Novel Potent, Selective, and Orally Active  
47  
48  
49  
50  
51  
52  
53  
54  
55  
56  
57  
58  
59  
60

1  
2  
3 Phosphodiesterase 2A Inhibitor, PDM-631. *Eur. J. Pharmacol.* **2017**, *811*, 110-116. (c) Gomez,  
4 L.; Massari, M. E.; Vickers, T.; Freestone, G.; Vernier, W.; Ly, K.; Xu, R.; McCarrick, M.;  
5  
6 Marrone, T.; Metz, M.; Yan, Y. G.; Yoder, Z. W.; Lemus, R.; Broadbent, N. J.; Barido, R.;  
7  
8 Warren, N.; Schmelzer, K.; Neul, D.; Lee, D.; Andersen, C. B.; Sebring, K.; Aertgeerts, K.;  
9  
10 Zhou, X.; Tabatabaei A.; Peters, M.; Breitenbucher, J. G. Design and Synthesis of Novel and  
11  
12 Selective Phosphodiesterase 2 (PDE2a) Inhibitors for the Treatment of Memory Disorders. *J.*  
13  
14 *Med. Chem.* **2017**, *60*, 2037-2051.

15  
16  
17  
18  
19  
20 7. Feng, B.; Mills, J. B.; Davidson, R. E.; Mireles, R. J.; Janiszewski, J. S.; Troutman, M. D.;  
21  
22 de Moraes, S. M., In Vitro P-glycoprotein Assays to Predict the In Vivo Interactions of P-  
23  
24 Glycoprotein with Drugs in the Central Nervous System. *Drug Metab. Dispos.* **2008**, *36*, 268-  
25  
26 275.

27  
28  
29  
30 8. Stepan, A. F.; Walker, D. P.; Bauman, J.; Price, D. A.; Baillie, T. A.; Kalgutkar, A. S.; Aleo,  
31  
32 M. D. Structural Alert/Reactive Metabolite Concept as Applied in Medicinal Chemistry to  
33  
34 Mitigate the Risk of Idiosyncratic Drug Toxicity: A Perspective Based on the Critical  
35  
36 Examination of Trends in the Top 200 Drugs Marketed in the United States. *Chem. Res. Toxicol.*  
37  
38 **2011**, *24*, 1345-1410.

39  
40  
41  
42 9. Haning, H.; Niewoehner, U.; Schenke, T.; Lampe, T.; Hillisch, A.; Bischoff, E. Comparison  
43  
44 of Different Heterocyclic Scaffolds as Substrate Analog PDE5 Inhibitors. *Bioorg. Med. Chem.*  
45  
46 *Lett.* **2005**, *15*, 3900-3907.

47  
48  
49  
50 10. Corbin, J. D.; Beasley, A.; Blount, M. A.; Francis, S. H. Vardenafil: Structural Basis for  
51  
52 Higher Potency Over Sildenafil in Inhibiting cGMP-Specific Phosphodiesterase-5 (PDE5).  
53  
54 *Neurochem. Int.* **2004**, *45*, 859-863.

1  
2  
3 11. Sung, B.-J.; Hwang, K. Y.; Jeon, Y. H.; Lee, J. I.; Heo, Y.-S.; Kim, J. H.; Moon, J.; Yoon,  
4 J. M.; Hyun, Y.-L.; Kim, E.; Eum, S. J.; Park, S.-Y.; Lee, J.-O.; Lee, T. G.; Ro, S.; Cho, J. M.  
5  
6 Structure of the Catalytic Domain of Human Phosphodiesterase 5 with Bound Drug Molecules.  
7  
8 *Nature* **2003**, *425*, 98-102.  
9

10  
11  
12  
13 12. For a PDE5A mutagenesis study that explored the role of different amino acids on the  
14 potency of **5** and **7**, see: Zoraghi, R.; Francis Sharron, H.; Corbin Jackie, D. Critical Amino  
15 Acids in Phosphodiesterase-5 Catalytic Site That Provide for High-Affinity Interaction with  
16 Cyclic Guanosine Monophosphate and Inhibitors. *Biochemistry* **2007**, *46*, 13554-13563.  
17  
18  
19

20  
21  
22  
23 13. Parlanti, L.; Discordia, R. P.; Hynes, J., Jr.; Miller, M. M.; O'Grady, H. R.; Shi, Z.,  
24 Amination of Heterocyclic Compounds with O-Benzoylhydroxylamine Derivatives. *Org. Lett.*  
25  
26 **2007**, *9*, 3821-3824.  
27  
28  
29

30  
31 14. Cocco, M. T.; Olla, C.; Onnis, V.; Schivo, M. L.; De Logu, A. 1-Acylaminoimidazoles  
32 Synthesis and Antimicrobial Activity, *Farmaco* **1993**, *47*, 229-238.  
33  
34  
35

36  
37 15. Edwards, M. P.; Price, D. A. Role of Physicochemical Properties and Ligand Lipophilicity  
38 Efficiency in Addressing Drug Safety Risks. *Annu. Rep. Med. Chem.* **2010**, *45*, 381-391.  
39  
40  
41

42 16. Pettersson, M.; Johnson, D. S.; Rankic, D. A.; Kauffman, G. W.; am Ende, C. W.; Butler,  
43 T. W.; Boscoe, B.; Evrard, E.; Helal, C. J.; Humphrey, J. M.; Stepan, A. F.; Stiff, C. M.; Yang,  
44 E.; Xie, L.; Bales, K. R.; Hajos-Korcsok, E.; Jenkinson, S.; Pettersen, B.; Pustilnik, L. R.;  
45  
46 Ramirez, D. S.; Steyn, S. J.; Wood, K. M.; Verhoest, P. R. Discovery of Cyclopropyl  
47 Chromane-Derived Pyridopyrazine-1,6-dione  $\gamma$ -Secretase Modulators with Robust Central  
48 Efficacy. *MedChemComm* **2017**, *8*, 730-743.  
49  
50  
51  
52  
53  
54  
55  
56  
57  
58  
59  
60

1  
2  
3 17. Shaffer, C. L.; Patel, N. C.; Schwarz, J.; Scialis, R. J.; Wei, Y.; Hou, X. J.; Xie, L.; Karki,  
4 K.; Bryce, D. K.; Osgood, S. M.; Hoffmann, W. E.; Lazzaro, J. T.; Chang, C.; McGinnis, D. F.;  
5  
6 Lotarski, S. M.; Liu, J.; Obach, R. S.; Weber, M. L.; Chen, L.; Zasadny, K. R.; Seymour, P. A.;  
7  
8 Schmidt, C. J.; Hajos, M.; Hurst, R. S.; Pandit, J.; O'Donnell, C. J., The Discovery and  
9  
10 Characterization of the  $\alpha$ -Amino-3-hydroxy-5-methyl-4-isoxazolepropionic Acid (AMPA)  
11  
12 Receptor Potentiator N-{(3S,4S)-4-[4-(5-Cyano-2-thienyl)phenoxy]tetrahydrofuran-3-  
13  
14 yl}propane-2-sulfonamide (PF-04958242). *Journal of Medicinal Chemistry* **2015**, *58*, 4291-  
15  
16 4308.  
17  
18  
19  
20

21  
22 18. Song, R. S.; Tolentino, R.; Sobie, E. A.; Neves-Zaph, S. R., Cross-Regulation of  
23  
24 Phosphodiesterase 1 and Phosphodiesterase 2 Activities Controls Dopamine-Mediated Striatal  $\alpha$ -  
25  
26 Amino-3-hydroxy-5-methyl-4-isoxazolepropionic Acid (AMPA) Receptor Trafficking. *J. Biol.*  
27  
28 *Chem.* **2016**, *291*, 23257-23267.  
29  
30

31  
32 19. Vijayraghavan, S.; Wang, M.; Birnbaum, S. G.; Williams, G. V.; Arnsten, A. F. T.,  
33  
34 Inverted-U Dopamine D1 Receptor Actions on Prefrontal Neurons Engaged in Working  
35  
36 Memory. *Nat. Neurosci.* **2007**, *10*, 376-384.  
37  
38

39  
40 20. Chen, L.; Nabulsi, N.; Naganawa, M.; Zasadny, K.; Skaddan, M. B.; Zhang, L.;  
41  
42 Najafzadeh, S.; Lin, S.-f.; Helal, C. J.; Boyden, T. L.; Chang, C.; Ropchan, J.; Carson, R. E.;  
43  
44 Villalobos, A.; Huang, Y., Preclinical Evaluation of 18F-PF-05270430, a Novel PET  
45  
46 Radioligand for the Phosphodiesterase 2A Enzyme. *J. Nucl. Med.* **2016**, *57*, 1448-1453.  
47  
48

49  
50 21. Di, L.; Rong, H.; Feng, B. Demystifying Brain Penetration in Central Nervous System  
51  
52 Drug Discovery. *J. Med. Chem.* **2013**, *56*, 2-12.  
53  
54

1  
2  
3 22. The targeted  $C_p$  was generated using the following data and approximations:  $C_{bu}$  for  
4 maximal reversal MK-801 in the cortical EEG assay was 9 nM (Table 7). As **30** is a Group I  
5 compound as described in reference 15,  $C_{bu} \sim C_{pu}$ . Adjusting for human plasma protein binding  
6 ( $f_{up} = 0.341$ ),  $C_p = 9 \text{ nM} / 0.341 = 26 \text{ nM}$ . Converting this value to ng/mL =  $26 \text{ nm/L} \times 414$   
7  
8 ng/nm / 1000 mL/L = 11 ng/mL.  
9  
10  
11  
12  
13

14  
15 23. Schmidt, C. J.; Chapin, D. S.; Cianfrogna, J.; Corman, M. L.; Hajos, M.; Harms, J. F.;  
16 Hoffman, W. E.; Lebel, L. A.; McCarthy, S. A.; Nelson, F. R.; Proulx-LaFrance, C.; Majchrzak,  
17 M. J.; Ramirez, A. D.; Schmidt, K.; Seymour, P. A.; Siuciak, J. A.; Tingley, F. D., III; Williams,  
18 R. D.; Verhoest, P. R.; Menniti, F. S. Preclinical Characterization of Selective  
19 Phosphodiesterase 10A Inhibitors: a New Therapeutic Approach to the Treatment of  
20 Schizophrenia. *J. Pharmacol. Exp. Ther.* **2008**, *325*, 681- 690.  
21  
22  
23  
24  
25  
26  
27  
28  
29  
30  
31  
32

33 Insert Table of Contents Graphic and Synopsis Here  
34  
35

